MASTER

Report No. BMI-1269
UC-81 Reactors - Power
(TID-4500 - 13th Ed., Rev.)

Contract No. W-7405-eng-92

SIMULATION OF VARIOUS ACCIDENT CONSIDERATIONS FOR A MERCHANT-SHIP PRESSURIZED-WATER REACTOR

by

Roger S. Boyd
Benjamin B. Gordon
Richard H. Byers
Leon E. Winslow
J. James Stone, Jr.

August 25, 1958

BATTELLE MEMORIAL INSTITUTE
505 King Avenue
Columbus 1, Ohio

DISCLAIMER

This report was prepared as an account of work sponsored by an agency of the United States Government. Neither the United States Government nor any agency Thereof, nor any of their employees, makes any warranty, express or implied, or assumes any legal liability or responsibility for the accuracy, completeness, or usefulness of any information, apparatus, product, or process disclosed, or represents that its use would not infringe privately owned rights. Reference herein to any specific commercial product, process, or service by trade name, trademark, manufacturer, or otherwise does not necessarily constitute or imply its endorsement, recommendation, or favoring by the United States Government or any agency thereof. The views and opinions of authors expressed herein do not necessarily state or reflect those of the United States Government or any agency thereof.

DISCLAIMER

Portions of this document may be illegible in electronic image products. Images are produced from the best available original document.

TABLE OF CONTENTS

SIMULATION OF VARIOUS ACCIDENT CONSIDERATIONS FOR A MERCHANT-SHIP PRESSURIZED-WATER REACTOR

Roger S. Boyd, Benjamin B. Gordon, Richard H. Byers,
Leon E. Winslow, and J. James Stone, Jr.

A study was conducted on the safety aspects of foreseeable accident types in connection with the Nuclear Merchant Ship Reactor program. Four accidents have been selected for analysis by analog simulation techniques: continuous rod withdrawal, startup, loss of coolant flow, and cold-water insertion.

The simulation of the reactor only was required for these situations because the effects of the accidents would be completed in less than one primary-coolant loop time. The external control system was ignored, and only the effects of the negative reactivity coefficients were considered in the natural shutdown of the plant.

Three phases of operation were considered in these analyses: operation with no safety system, high-flux scram, and period scram. The programs involved the variations of the scram parameters and the reactor temperature coefficients over the range of possible values for this reactor power plant.

Results indicate that the inherent stability of the reactor system is sufficient to attenuate the power excursions resulting from the first three accidents. In the cold-water accident, if the difference in loop temperatures is on the order of 300 F, scram is necessary to limit the power excursion.

INTRODUCTION

The NMSR program is concerned with the design and construction of the first nuclear merchant ship, the NS "Savannah". Prime contractor for the design and construction of the propulsion plant is The Babcock & Wilcox Company. The reactor power plant specified is of the pressurized-water type, rated at 74 megawatts. Control of the plant is to be accomplished through use of a control-rod drive mechanism. Present indications are that this system will use a constant-average-temperature program.(1)

This report outlines the analyses made at the request of The Babcock & Wilcox Company of the response of the Nuclear Merchant Ship Reactor to four accident conditions: (1) continuous rod withdrawal, (2) startup, (3) loss of coolant flow, and (4) cold-water insertion. The results of these analyses will be included in the over-all safety report which The Babcock & Wilcox Company will submit to the AEC Safeguards Committee for approval. All input information has been provided by The Babcock & Wilcox Company.

This investigation was carried out using analog simulation techniques. In each case the accident situation was completely specified and remained fixed. The programs involved the variations of the scram parameters and the reactor temperature coefficients over the range of possible values for this reactor power plant.

(1) References at end.

DESCRIPTION OF THE REACTOR POWER PLANT

The reactor power plant to be used in the merchant ship is of the pressurized-water type.[2] The system has two primary-coolant loops, each with its own steam generator. This equipment, plus the pressurizer and control and instrumentation systems, is located in a containment vessel approximately 50 ft long and 35 ft in diameter.

The primary cooling system operates at a constant pressure of 1750 psi and a mean reactor water temperature of 508 F. Power ratings of the reactor are 63, 69, and 74 megawatts, corresponding to normal rate of operation, maximum rate of operation, and maximum design point, respectively.

The reactor pressure vessel is a cylindrical shell with hemispherical bottom and spherical dished top. The control-rod drives are located at the top of the reactor. Water flows through the reactor in three passes: (1) it enters near the bottom of the reactor and flows up through the thermal shields, (2) it flows down through the outer portion of the core, and (3) it flows up through the center of the core and out through the top of the reactor. A diagrammatic representation of the reactor, primary-coolant loop, and boiler is shown in Figure 1. Since less than 1 per cent of the power is generated in the thermal shields, the heat produced by this portion of the system was neglected for simulation purposes. It was estimated that, of the total heat generated in the system, 27.5 per cent is generated in the second pass, and 72.5 per cent is generated in the third pass.

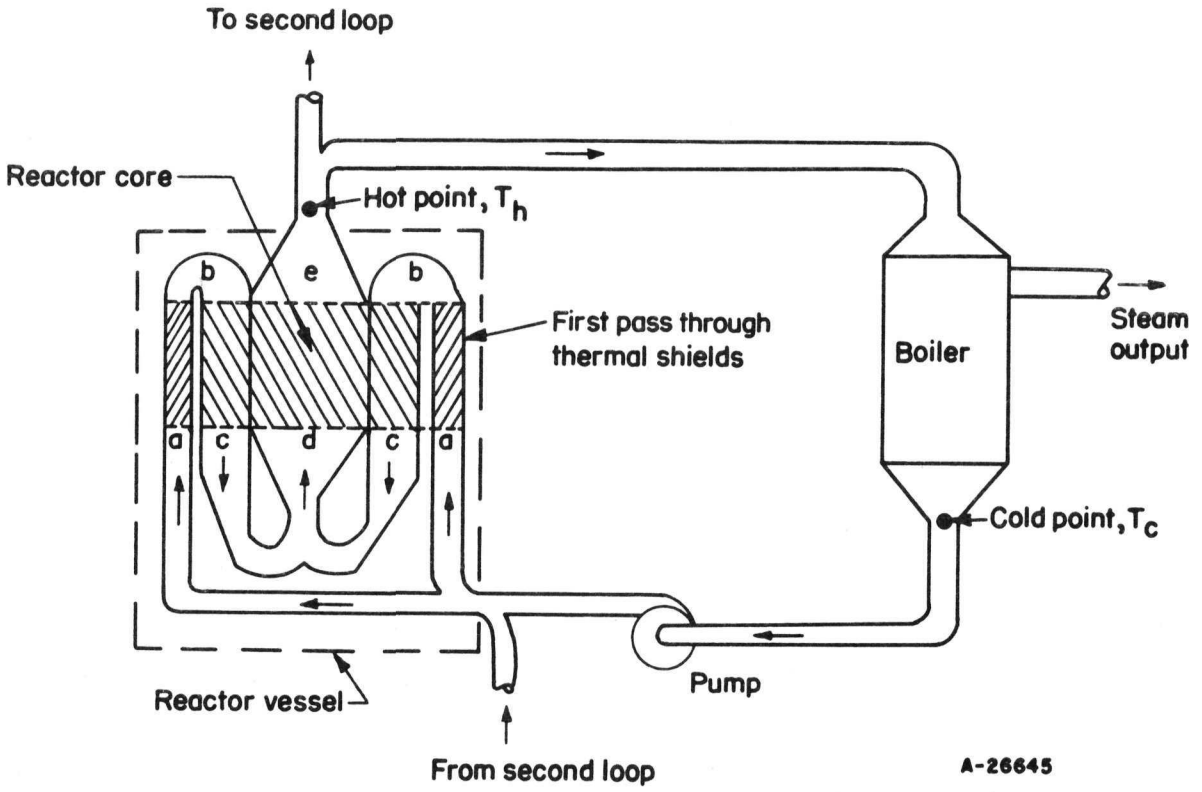

FIGURE 1. REACTOR POWER-PLANT SYSTEM SCHEMATIC

The core consists of 32 elements with 180 fuel pins per element. The fuel pins are right-circular cylinders of UO_2, placed in a stainless steel cladding with helium between the UO_2 and the steel. It was assumed that the geometry of the fuel pins would not vary with temperature transients.

Heat is transferred from the reactor to the two boilers by means of pressurized water flowing through two parallel loops. The purpose of pressurizing the system is to prevent boiling of the water in the reactor loop.

There are two water pumps in parallel in each loop located downstream from the steam generator. It is possible for the propulsion plant to operate on one loop only. The effect of accidentally starting up the cold loop is the topic of the fourth accident study.

In general, the resulting scram after each accident will take place within one loop time. Therefore, the simulation will involve the reactor only. The primary-coolant loop with the boiler has been neglected as have the auxiliary systems of the power plant: pressurizer, purification, and intermediate cooling systems. The control system has been considered inoperative. Any variations in this simulation will be discussed in the sections dealing with the accident to which they pertain.

SIMULATION OF THE REACTOR

The reactor simulation was developed by first constructing a block diagram of the system (Figure 2). The individual components were then analyzed to determine their specific function, and a computer diagram was produced which satisfied these functions. From the computer diagram, equations were written which described the system.

The following sections of this report describe the simulation of the various components of the system. The locations of the various simulated components are as shown in Figure 1.

Nuclear Kinetic Equations

Standard nuclear kinetic equations were employed in the study of this reactor. These are:

$$\frac{dP_r}{dt} = \left[\frac{(1 - \beta)\, k - 1}{\ell}\right] P_r + \sum_{i=1}^{i=6} \lambda_i C_i + S_o \quad , \tag{1}$$

$$\frac{dC_i}{dt} = -\lambda_i C_i + \frac{\beta_i k}{\ell} P_r \quad , \tag{2 to 7}$$

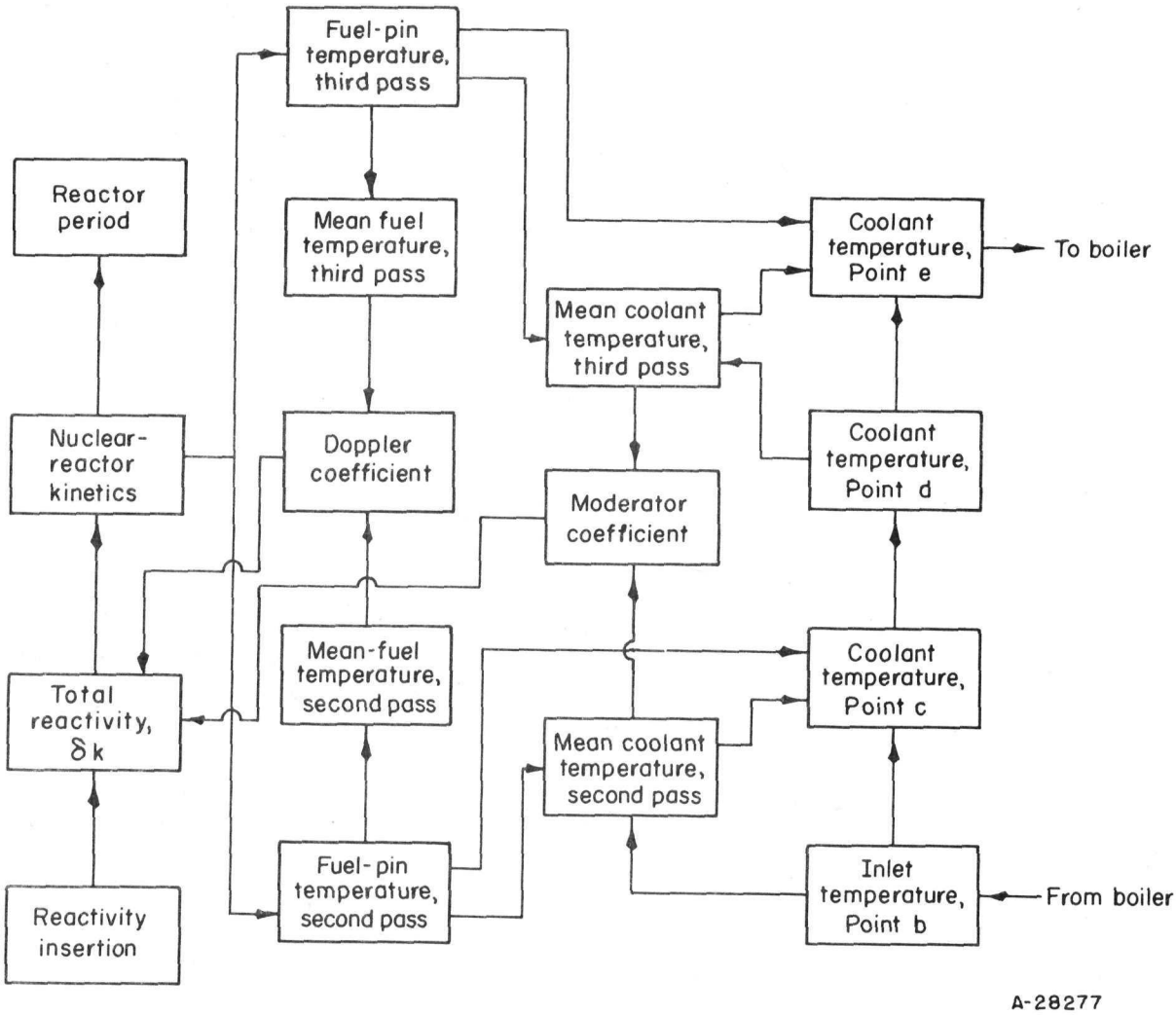

FIGURE 2. BLOCK DIAGRAM OF REACTOR SYSTEM

where

P_r = reactor power, Btu per sec

$\beta = \sum_{i=1}^{i=6} \beta_i$

β_i = fraction of neutrons produced each mean lifetime that are delayed in the ith group

ℓ = mean lifetime, 2.7×10^{-5} sec

λ_i = decay constant for ith delay group, per sec

S_o = term proportional to neutron source

C_i = term proportional to concentration of ith delay group

k = effective multiplication factor.

The Battelle Analog Facility has a self-contained Nuclear Kinetic Feedback Unit to solve these equations. The use of this unit requires only two operational amplifiers and saves considerable setup time. A description of a similar unit can be found in ORNL-1632[3].

This unit was used in this investigation where possible. The values of λ_i and β_i for the six delay groups used in this simulation are listed in Table 1.

TABLE 1. DELAYED-NEUTRON DATA

Group	Decay Constant, λ_i, per sec	Delayed-Neutron Fraction, β_i
1	0.0124	0.00026
2	0.0315	0.00170
3	0.151	0.00219
4	0.465	0.00254
5	1.61	0.00092
6	13.86	0.00025
	Total	0.00786

Fuel-Pin Temperatures

The simulation of the heat-transfer characteristics of the fuel pins involves the solution of the equation of radial heat flow with cylindrical geometry. Partial differential equations of this type are not suited for solution on an analog computer, and must be rewritten using ordinary differential equations. The technique most often used is the application of finite differences. The heat-transfer medium is divided into a number of small sections, and equations relating the differences of the average temperatures of these sections are written.

In this study the fuel pin was divided into seven sections: five UO_2, one helium, and one stainless steel. Figure 3 shows the geometry of the cylindrical fuel pin and the division of the pin into finite boundaries to facilitate study of the radial-heat-flow characteristics on an analog computer. In the following description, let

r = radial distance, in.

c = specific heat, Btu/(lb)(F)

ρ = density, lb per in.^{3}

θ = temperature, F

k = thermal conductivity, Btu/(sec)(in.)(F)

q = heat generated in the fuel, Btu/(sec)(in.^{3}).

A "pie" slice was taken from the cylinder and divided as shown in Figure 4. Writing the finite-differences equations of heat transfer radially through the slice involves the cross-sectional area at the interface of two sections and the volume of each section. The finite-differences equations for this geometry for the time derivatives of temperature are as follows:

$$c_1\rho_1 V_1\dot{\theta}_1 = -\frac{k_{12}}{\Delta r_{12}} A_{12}(\theta_1 - \theta_2) + qV_1 , \tag{8}$$

$$c_2\rho_2 V_2\dot{\theta}_2 = -\frac{k_{23}}{\Delta r_{23}} A_{23}(\theta_2 - \theta_3) + \frac{k_{12}}{\Delta r_{12}} A_{12}(\theta_1 - \theta_2) + qV_2 , \tag{9}$$

$$c_3\rho_3 V_3\dot{\theta}_3 = -\frac{k_{34}}{\Delta r_{34}} A_{34}(\theta_3 - \theta_4) + \frac{k_{23}}{\Delta r_{23}} A_{23}(\theta_2 - \theta_3) + qV_3 , \tag{10}$$

$$c_4\rho_4 V_4\dot{\theta}_4 = -\frac{k_{45}}{\Delta r_{45}} A_{45}(\theta_4 - \theta_5) + \frac{k_{34}}{\Delta r_{34}} A_{34}(\theta_3 - \theta_4) + qV_4 , \tag{11}$$

$$c_5\rho_5 V_5\dot{\theta}_5 = -\frac{k_{56}}{\Delta r_{56}} A_{56}(\theta_5 - \theta_{He}) + \frac{k_{45}}{\Delta r_{45}} A_{45}(\theta_4 - \theta_5) + qV_5 , \tag{12}$$

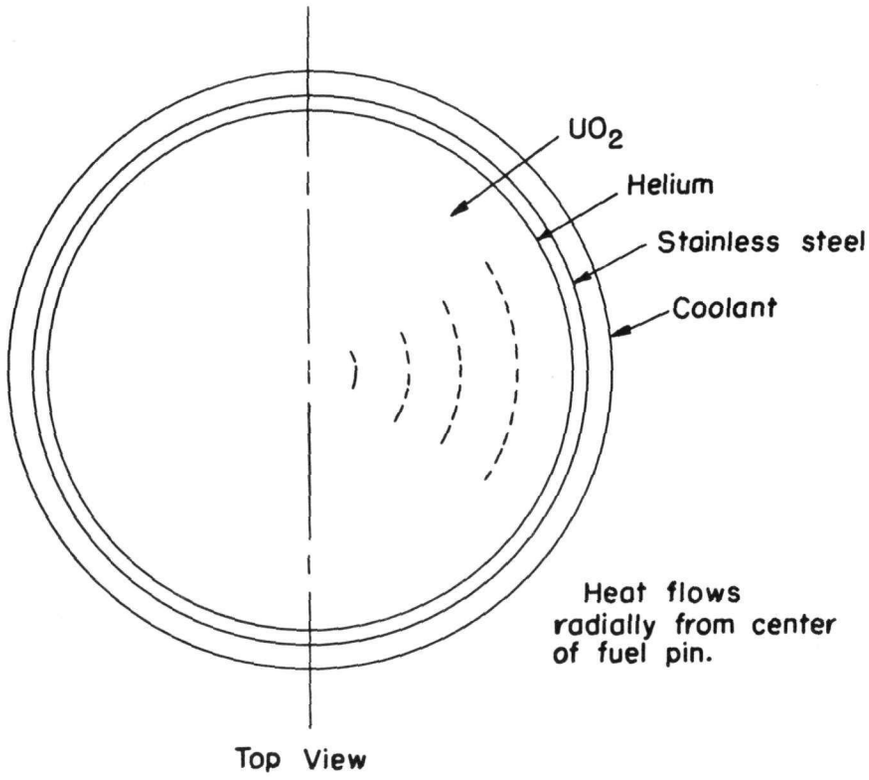

Pin is divided into five sections of UO_2, one section of helium, and one section of stainless steel

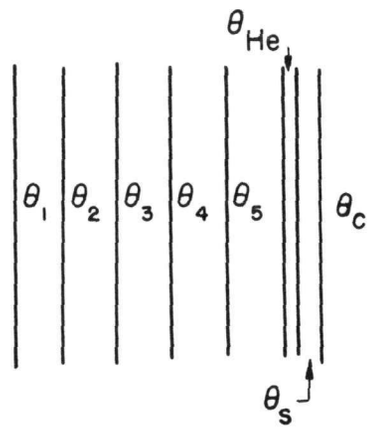

FIGURE 3. GEOMETRY OF FUEL PIN

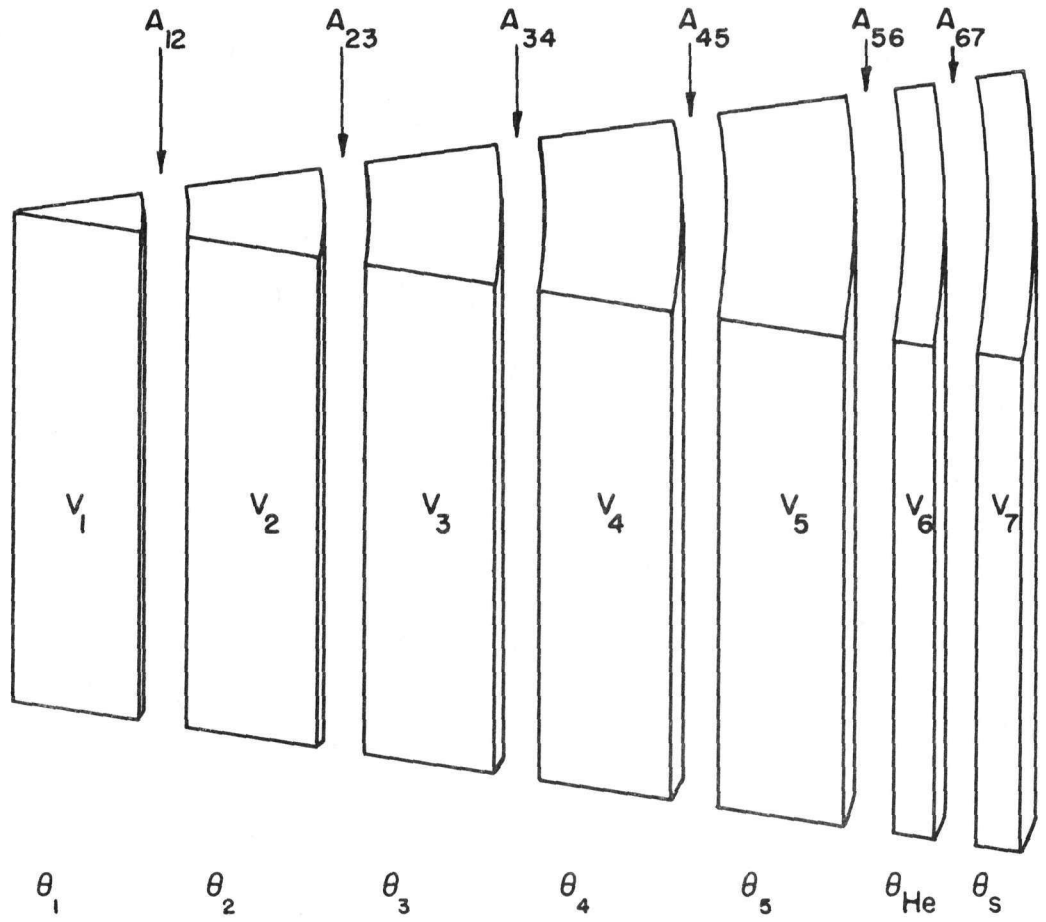

Frontal heat-transfer area and volume of seven-section fuel pin as shown

FIGURE 4. "PIE" SLICE OF FUEL PIN

$$c_6\rho_6V_6\dot{\theta}_{He} = -\frac{k_{67}}{\Delta r_{67}}A_{67}(\theta_{He} - \theta_s) + \frac{k_{56}}{\Delta r_{56}}A_{56}(\theta_5 - \theta_{He}), \quad (13)$$

$$c_7\rho_7V_7\dot{\theta}_s = -\frac{k_{78}}{\Delta r_{78}}A_{78}(\theta_s - \theta_c) + \frac{k_{67}}{\Delta r_{67}}A_{67}(\theta_{He} - \theta_s), \quad (14)$$

where

V_1 = volume of first section; V_2 = volume of second section, etc., in.^{3}

A_{12} = cross-sectional area between first and second sections; A_{23} = cross-sectional area between second and third sections; etc., in.^{2}

Δr_{12} = radial distance between centers of first and second sections; Δr_{23} = radial distance between the centers of second and third sections; etc., in.

k_{12} = thermal conductivity of Sections 1 and 2; k_{23} = thermal conductivity of Sections 2 and 3; etc., Btu/(sec)(in.)(F).

The subscripts to c, ρ, θ, and $\dot{\theta}$ refer to the sections to which these quantities pertain.

Since $\frac{k_{56}}{\Delta r_{56}}$, $\frac{k_{67}}{\Delta r_{67}}$, and $\frac{k_{78}}{\Delta r_{78}}$ involve the thermal conductivities of two different materials, some special attention must be given these quantities. Figure 5 is a cross-sectional view of Sections 5 and 6.

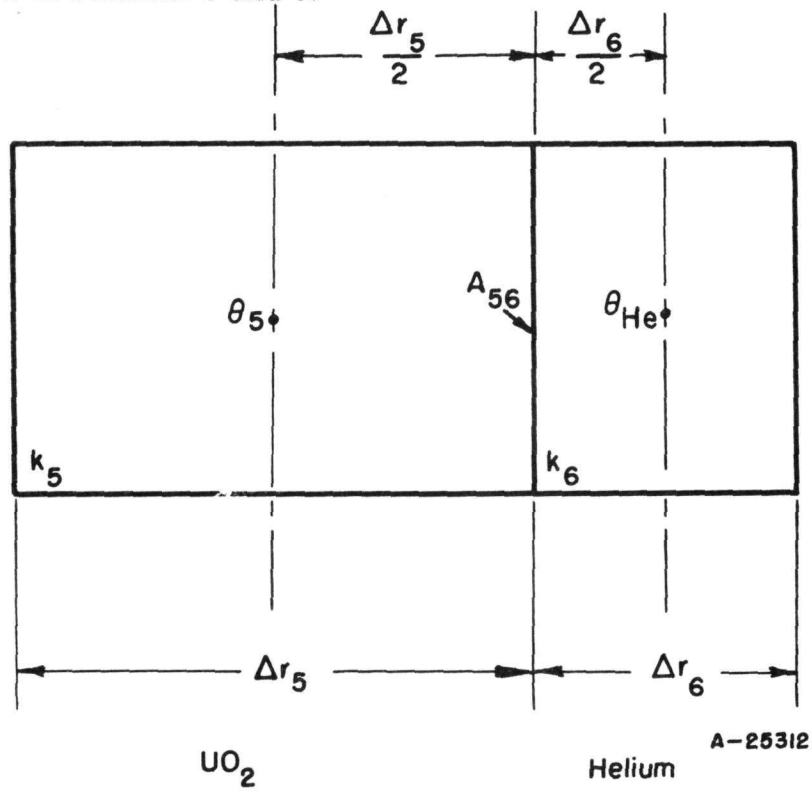

FIGURE 5. CROSS-SECTIONAL VIEW OF SECTIONS 5 AND 6

The thermal conductance in the half of Section 5 adjacent to Section 6 is equal to

$$\frac{k_5}{\Delta r_5/2}\, A_{56} .$$

Therefore, the resistance to heat flow in this portion of Section 5 is equal to

$$\frac{\Delta r_5}{2k_5 A_{56}} .$$

Similarly, the resistance to heat flow in the half of Section 6 adjacent to Section 5 is equal to

$$\frac{\Delta r_6}{2k_6 A_{56}} .$$

The total resistance from the center of Section 5 to the center of Section 6 is equal to

$$\frac{\Delta r_5}{2k_5 A_{56}} + \frac{\Delta r_6}{2k_6 A_{56}} .$$

Therefore, the thermal conductance in this portion of the system is equal to

$$\frac{2k_5 k_6 A_{56}}{k_6 \Delta r_5 + k_5 \Delta r_6} .$$

This must be equal to the expression in Equations (12) and (13):

$$\frac{k_{56}}{\Delta r_{56}}\, A_{56} .$$

Therefore,

$$\frac{k_{56}}{\Delta r_{56}} = \frac{2k_5 k_6}{k_6 \Delta r_5 + k_5 \Delta r_6} .$$

Similarly,

$$\frac{k_{67}}{\Delta r_{67}} = \frac{2k_6 k_7}{k_7 \Delta r_6 + k_6 \Delta r_7} .$$

and

$$\frac{k_{78}}{\Delta r_{78}} = \frac{2k_7 k_8}{k_8 \Delta r_7 + 2k_7} .$$

These values of thermal conductance were substituted into Equations (12), (13), and (14). The subscripts a, b, c, and d, referring to the UO_2, helium, stainless steel,

and coolant film, respectively, were used to replace the numerical subscripts of c, ρ, k, and Δr. The values of V and A were substituted into Equations (8) through (14).

Equations (15) through (21) were obtained by dividing through by V and simplifying. These equations are as follows:

$$c_a\rho_a\dot{\theta}_1 = -2\frac{k_a}{\Delta r_a^2}(\theta_1 - \theta_2) + q, \tag{15}$$

$$c_a\rho_a\dot{\theta}_2 = -\frac{4}{3}\frac{k_a}{\Delta r_a^2}(\theta_2 - \theta_3) + \frac{2}{3}\frac{k_a}{\Delta r_a^2}(\theta_1 - \theta_2) + q, \tag{16}$$

$$c_a\rho_a\dot{\theta}_3 = -\frac{6}{5}\frac{k_a}{\Delta r_a^2}(\theta_3 - \theta_4) + \frac{4}{5}\frac{k_a}{\Delta r_a^2}(\theta_2 - \theta_3) + q, \tag{17}$$

$$c_a\rho_a\dot{\theta}_4 = -\frac{8}{7}\frac{k_a}{\Delta r_a^2}(\theta_4 - \theta_5) + \frac{6}{7}\frac{k_a}{\Delta r_a^2}(\theta_3 - \theta_4) + q, \tag{18}$$

$$c_a\rho_a\dot{\theta}_5 = -\frac{20}{9}\frac{k_ak_b}{\Delta r_a^2k_b + \Delta r_a\Delta r_bk_a}(\theta_5 - \theta_6) + \frac{8}{9}\frac{k_a}{\Delta r_a^2}(\theta_4 - \theta_5) + q, \tag{19}$$

$$c_b\rho_b\dot{\theta}_{He} = -2\frac{k_bk_c}{\Delta r_b^2k_c + \Delta r_b\Delta r_ck_b}(\theta_{He} - \theta_s) + 2\frac{k_ak_b}{\Delta r_a\Delta r_bk_b + \Delta r_b^2k_a}(\theta_5 - \theta_{He}), \tag{20}$$

$$c_c\rho_c\dot{\theta}_s = -\frac{k_ck_d}{\Delta r_ck_c + k_d\frac{\Delta r_c^2}{2}}(\theta_s - \theta_c) + 2\frac{k_bk_c}{\Delta r_b\Delta r_ck_c + \Delta r_c^2k_b}(\theta_{He} - \theta_s). \tag{21}$$

This system was linearized by assuming the specific heats and thermal conductivities to be constant over the range of temperatures involved. This is an approximation, since the specific heat and thermal conductivity do vary with temperature.

The system was originally studied using the thermal conductivity of UO_2 at 2000 F to obtain approximate steady-state temperatures of the five sections of UO_2. These temperatures ranged from 1410 to 815 F. Successive iterations produced the temperatures and corresponding conductivities listed in Table 2. These are the steady-state temperatures with the plant operating at 74 megawatts.

TABLE 2. THERMAL CONDUCTIVITIES OF UO_2

Variable	Temperature, F	Thermal Conductivity, 10^{-5} Btu/(sec)(in.)(F)
	Second Pass	
θ_{2_1}	705	5.014
θ_{2_2}	691	5.132
θ_{2_3}	663	5.326
θ_{2_4}	626	5.660
θ_{2_5}	578	5.808
	Third Pass	
θ_{3_1}	1115	3.672
θ_{3_2}	1070	3.834
θ_{3_3}	973	4.134
θ_{3_4}	853	4.636
θ_{3_5}	700	5.003

The equation for the average fuel temperature, each pass, is the sum of these temperatures, weighted according to the volume represented in each section. Thus:

$$\theta_f = 0.0400\,\theta_1 + 0.1206\,\theta_2 + 0.2108\,\theta_3 + 0.2689\,\theta_4 + 0.3597\,\theta_5 \quad . \tag{22}$$

The input to this system, the heat per unit volume generated in the UO_2, was 0.6617 Btu/(sec)(in.^{3}) in the second pass, and 1.744 Btu/(sec) (in.^{3}) in the third pass. It was assumed that these amounts were generated uniformly throughout each of the five sections of the fuel pins.

The computer diagram used to represent this system is shown in Figure 6.* This diagram was developed from Equations (15) through (21) by standard mechanization and scaling techniques.

*Operational amplifiers, represented by a triangle in the computer diagram, have an inherent polarity reversal. Thus, a positive input will result in a negative output.

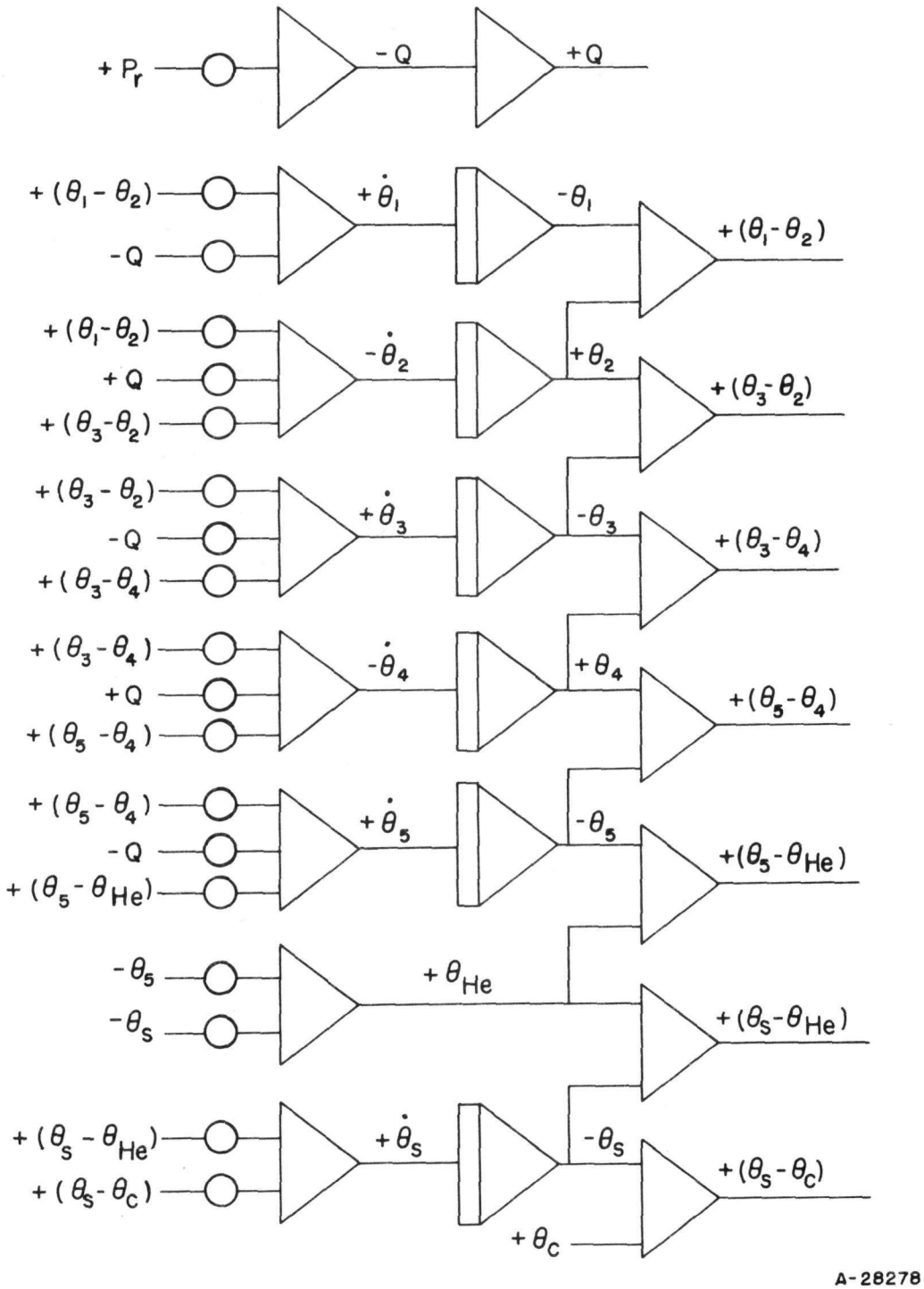

FIGURE 6. FUEL-PIN SIMULATION

The time constant of the integrator used to simulate the helium temperature was very short. It was decided that this integrator could be replaced satisfactorily by a standard summer. This implies that $c_6\rho_6\dot{\theta}_{He}$ is very small compared with the other terms in Equation (20) which can now be rewritten as follows:

$$\left[\frac{k_b k_c}{\Delta r_b{}^2 k_c + \Delta r_b \Delta r_c k_b} + \frac{k_a k_b}{\Delta r_a \Delta r_b k_b + \Delta r_b{}^2 k_a}\right] \theta_{He}$$

$$= \left[\frac{k_a k_b}{\Delta r_a \Delta r_b k_b + \Delta r_b{}^2 k_a}\right] \theta_5 + \left[\frac{k_b k_c}{\Delta r_b{}^2 k_c + \Delta r_b \Delta r_c k_b}\right] \theta_s \, . \qquad (23)$$

The coolant film coefficients, k_d, for each of the flow rates considered in this simulation are listed in Table 3. The rest of the constants are in Table 4.

TABLE 3. COOLANT FILM COEFFICIENTS

Percentage of Full Flow	Coolant Film Coefficient, k_d, 10^{-3} Btu/(sec)(in.^{2})(F)	
	Second Pass	Third Pass
100	6.819	6.256
83.1	5.883	5.397
63.7	4.754	4.361
57.6	4.386	4.024
33.4	2.836	2.602

These coefficients were computed from

$$h/h_o = (W/W_o)^{+0.8} \, , \qquad (24)$$

where W_o equals full flow, and h_o equals the film coefficient corresponding to W_o.

In all temperatures throughout this simulation, the reference level (zero volts) was taken as the mean coolant temperature, 508 F.

Reactor-Coolant Temperatures

Temperatures in the primary loop have been designated T_{i_j} or T_{i_k}, and temperatures in the reactor core have been designated θ_{i_j} or θ_{i_k}, where i indicates the type

TABLE 4. FUEL-PIN CONSTANTS

Materials	Quantity	Value
UO_2	C_a	0.0746 Btu/(lb) (F)
	ρ_a	0.2977 lb per in.^{3}
	Δr_a	0.0442 in.
Helium	k_b	3.87×10^{-6} Btu/(sec)(in.)(F)
	C_b	1.24 Btu/(lb)(F)
	ρ_b	6.447×10^{-6} lb per in.^{3}
	Δr_b	0.003 in.
Stainless steel	k_c	2.701×10^{-4} Btu/(sec)(in.)(F)
	C_c	0.12 Btu/(lb)(F)
	ρ_c	0.2799 lb per in.^{3}
	Δr_c	0.026 in.

of temperature, such as coolant, steel, helium, fuel, etc., and j or k represents the location as indicated in Figures 1 and 2. For mean temperatures, both j and k are used to indicate the two locations for which the mean is taken.

The simulation of the mean-coolant and coolant outlet temperatures was based upon the analysis found in ORNL-1632.

Let

P_z = design-point power per pass, Btu per sec

C_{ss} = total heat capacity of the steel per pass, Btu per F

Z_1 = design-point difference between coolant temperature and pin temperature, F

Z_2 = design-point rise in coolant temperature, F

τ_1 = transit time of coolant through the reactor, sec

$\theta_{c_{jk}}$ = mean coolant temperature, F

T_{c_j} = coolant inlet temperature, F

T_{c_k} = coolant outlet temperature, F

R_s = time constant of steel cladding, sec

ΔT = temperature differential through the reactor, F.

The following relationships exist among these constants:

(1) $Z_1 = R_s P_z / C_{ss}$

(2) Z_2 = % P_z of total P_r times ΔT.

Table 5 lists the values of these constants for the second and third passes. The mean inlet temperature is 495 F, and the mean outlet temperature is 521 F. Thus, ΔT of the reactor equals 26 F at full flow.

TABLE 5. DESIGN-POINT VALUES OF CONSTANTS FOR THE REACTOR-COOLANT-TEMPERATURE SIMULATION

	Second Pass	Third Pass
P_z, Btu per sec	19,293	50,863
C_{ss}, Btu per F	248	248
R_s, sec	0.1405	0.1542
τ_1, sec	0.546	0.610
Z_1, F	16	40
Z_2, F	7.15	18.85

The equation describing the generation of the mean coolant temperature is:

$$\dot{\theta}_{c_{jk}} = \frac{Z_2}{Z_1 \tau_1}\left(\theta_{s_j} - \theta_{c_{jk}}\right) - \frac{2}{\tau_1}\left(\theta_{c_{jk}} - T_{c_j}\right) \tag{25}$$

The outlet temperature of the coolant leaving the reactor is proportional to the delayed (by τ_1) inlet temperature and also to the integral of temperature difference between the steel and coolant. The transport lag of the coolant is approximated by two linear first-order delays.

The contribution to $\dot{T}_{c_k}$ equal to the heat added to the system is:

$$\frac{2 Z_2}{\tau_1 Z_1}\left(\theta_{s_j} - \theta_{c_{jk}}\right) .$$

The delayed contributions, with $\theta_{c_{jk}}$ temperature variation through the section of the reactor considered, are expressed as:

$$(\tau_1/2)\ \dot{\theta}_{c_{jk}} + \theta_{c_{jk}} = T_{c_j} , \tag{26}$$

$$(\tau_1/2)\ \dot{T}_{c_k} + T_{c_k} = \theta_{c_{jk}} . \tag{27}$$

Therefore,

$$T_{c_k} = \frac{Z_2}{Z_1}\left(\theta_{s_j} - \theta_{c_{jk}}\right)\left[\frac{1}{(\tau_1/2)\ S + 1}\right] + \left[\frac{1}{(\tau_1/2)\ S + 1}\right]^2 T_{c_j} . \tag{28}$$

Figure 7 is the computer diagram used in this portion of the simulation. The various reactor-coolant temperatures involved are listed and described in Table 6.

Since the inlet temperature to the second pass, T_{c_b}, was represented as a constant, the RC delay network became a constant resistance equal to $\tau_1/2$.

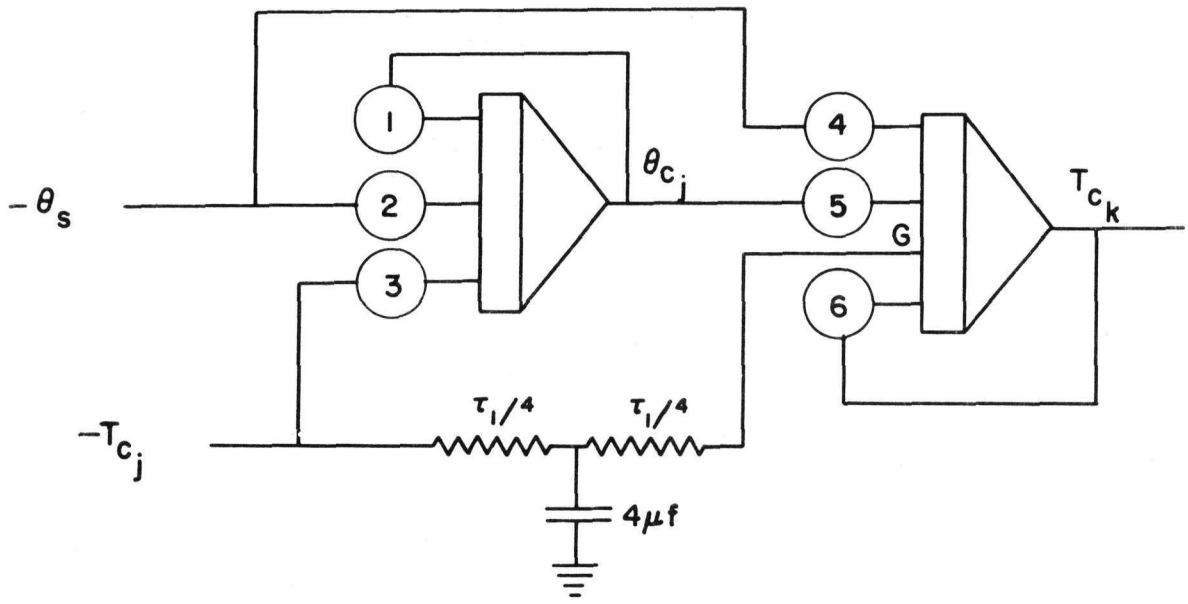

1. $\frac{Z_2}{\tau_1 Z_1} + \frac{2}{\tau_1}$

2. $\frac{Z_2}{\tau_1 Z_1}$

3. $2/\tau_1$

4. $\frac{2Z_2}{\tau_1 Z_1}$

5. $\frac{2Z_2}{\tau_1 Z_1}$

6. $2/\tau_1$

A-26646

FIGURE 7. COMPUTER DIAGRAM FOR REACTOR-COOLANT TEMPERATURES

TABLE 6. COOLANT REACTOR TEMPERATURES DESCRIPTION

Temperature	Description
T_{c_b}	Inlet temperature to second pass
$\theta_{c_{bc}}$	Mean coolant temperature, second pass
T_{c_c}	Outlet temperature from second pass
T_{c_d}	Inlet temperature to third pass
$\theta_{c_{de}}$	Mean coolant temperature, third pass
T_{c_e}	Outlet temperature from third pass

Coolant-Temperature-Transport Delays

The lag times in the second and third passes were approximated by cascading two first-order delays. The transport delay of the coolant flowing between the two passes, T_{c_c} to T_{c_d}, was simulated using an eight-root network.[4] This simulation is shown in Figure 8.

One of the parameters in the system analysis is the flow rate. Table 7 shows the maximum power level as a function of the various flow rates. The flow rate is determined by the number of pumps operating in the two coolant loops.

The transport delay times corresponding to these flow rates are presented in Table 8 along with the lag times in the two passes.

TABLE 7. MAXIMUM POWER LEVEL AS A FUNCTION OF FLOW RATE

Power, megawatts	Percentage of Maximum Power	Percentage of Full Flow for Indicated Number of Pumps in Operation				
		4	3	2 (2 Loops)	2 (1 Loop)	1
74.0	100	100				
60.7	82		83.1			
45.1	61			63.7		
40.0	54				57.6	
20.0	27					33.4
7.4	10					33.4

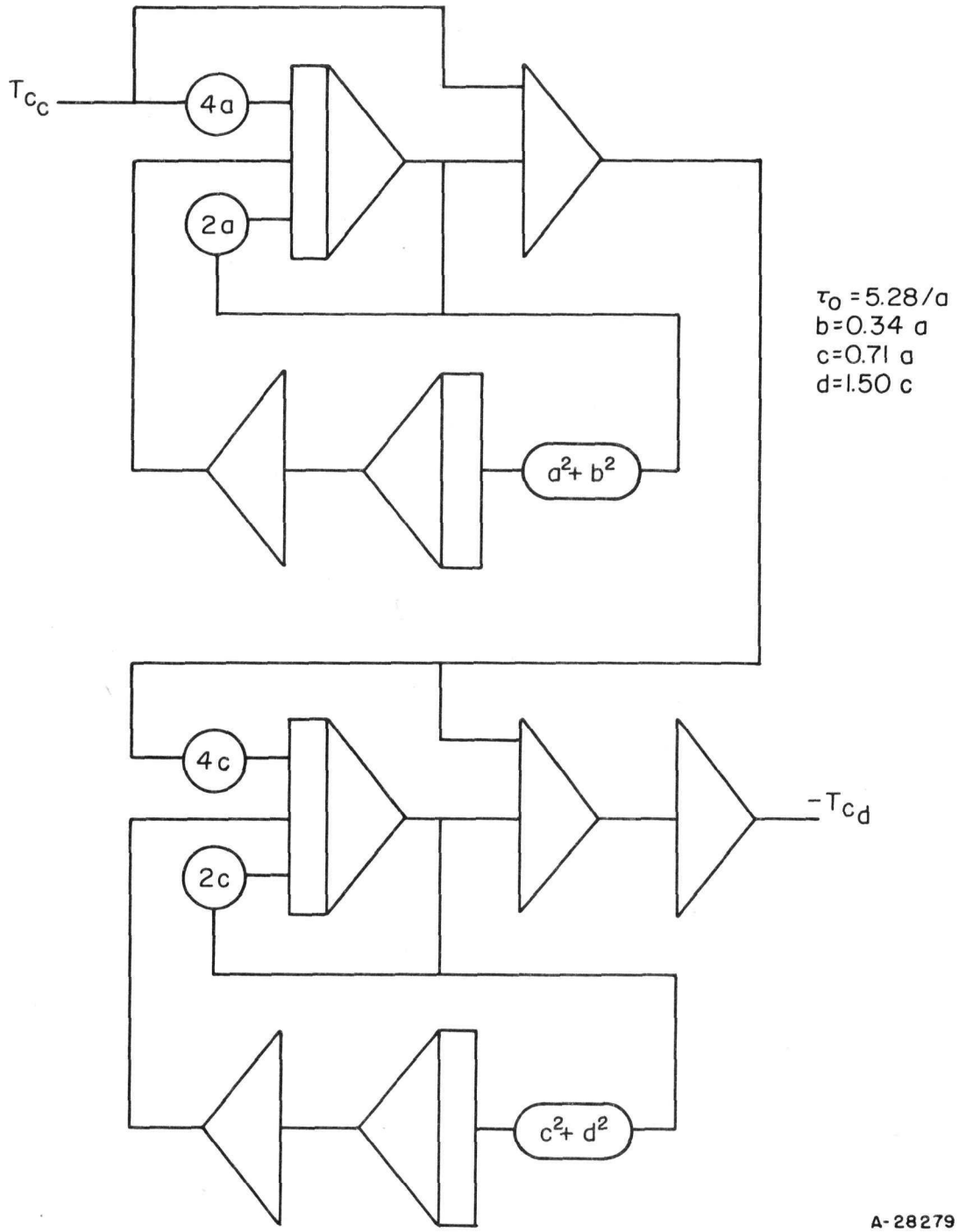

FIGURE 8. COOLANT-TRANSPORT-DELAY SIMULATION

TABLE 8. TRANSPORT DELAY TIMES IN THE REACTOR AS A FUNCTION OF COOLANT-FLOW RATE

Flow, 10^6 lb per hr	Percentage of Full Flow	Delay Time, sec		
		Second Pass	Between Passes	Third Pass
8.000	100	0.546	3.007	0.601
6.648	83.1	0.657	3.619	0.734
5.096	63.7	0.857	4.721	0.958
4.608	57.6	0.948	5.220	1.059
2.672	33.4	1.635	9.003	1.826

A block diagram of the thermal loop is shown in Figure 9. Values of the inlet temperature corresponding to the various combinations of power level and flow rate are listed in Table 9.

Initially the system was observed under all standard operating conditions. The resultant steady-state temperatures, corresponding to Figure 9, are shown in Table 10.

Reactor Temperature Coefficients and Reactivity

The reactivity, ρ, is given as the ratio $\delta k/k$, which is approximately equal to δk for small δk's. This assumption has been made in these simulation studies.

The negative temperature coefficients of reactivity represent the inherent stability of this reactor. Two specific coefficients were considered: the moderator coefficient and the Doppler coefficient. The former is a function of reactor mean coolant temperature, while the latter is a function of the fuel temperature due to the change in resonance escape probability. In this term, the temperature coefficient of reactivity is attributed to "Doppler broadening" of resonance peaks in the neutron spectrum. In general, the larger the negative coefficients, the smaller the power excursions following a disturbance. However, with the existence of a large Doppler coefficient, the average system temperature tends to fluctuate considerably from its design point when the plant is subjected to load changes.

The range of values of these coefficients used in this simulation is presented in Table 11.

Figure 10 represents the computer diagram showing the coupling of the reactor temperatures to the reactivity expression. This may be referred to as the internal reactor control loop.

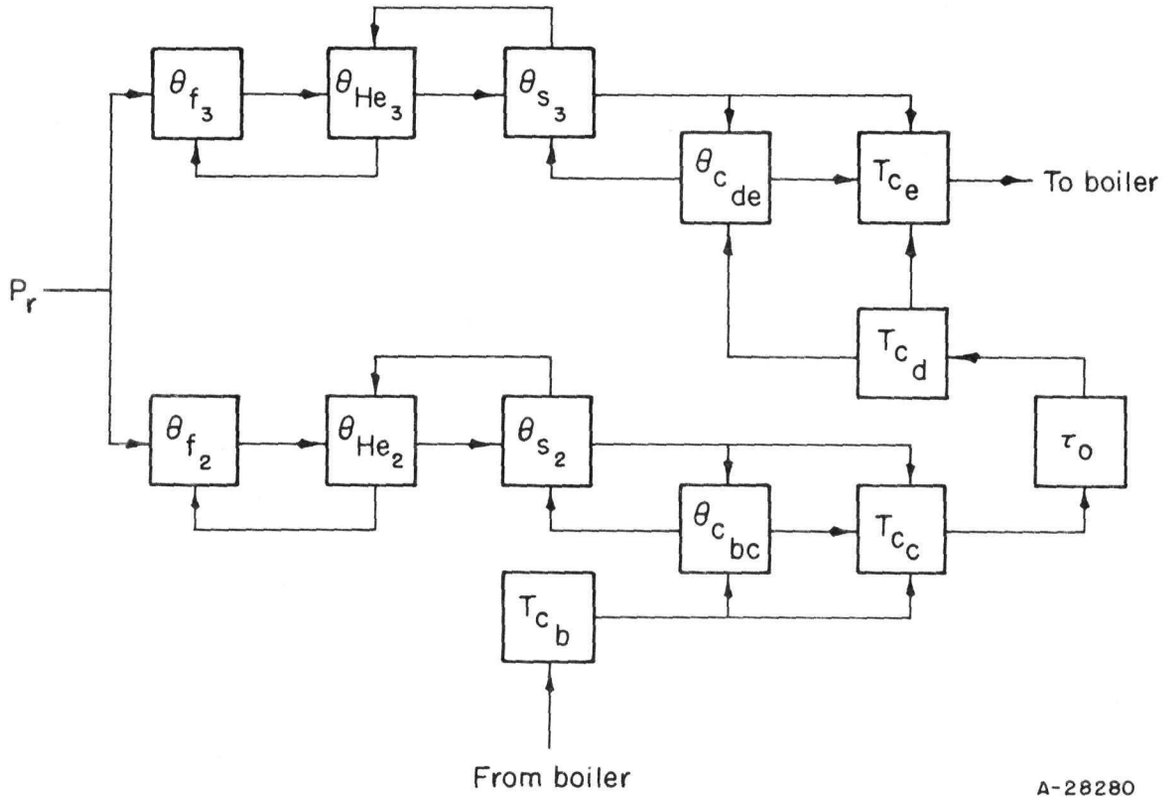

FIGURE 9. BLOCK DIAGRAM OF THE THERMAL LOOP

TABLE 9. REACTOR-COOLANT INLET TEMPERATURES AND ΔT ACROSS THE REACTOR FOR THE VARIOUS COMBINATIONS OF POWER AND FLOW

Percentage of Power	Percentage of Full Flow	ΔT, F	Inlet Temperature, F
100	100	26	495
100	83.1	31.3	492.4
82	100	21.3	497.4
82	83.1	25.7	495.2
61	100	15.9	500.0
61	83.1	19.1	498.4
61	63.7	24.9	495.6
61	57.6	27.5	494.2
54	100	14.0	501.0
54	83.1	16.9	499.6
54	63.7	22.0	497.0
54	57.6	24.4	495.8
27	100	7.0	504.5
27	83.1	8.5	503.8
27	63.7	11.0	502.5
27	57.6	12.2	501.9
27	33.4	21.0	497.5
10	100	2.6	506.7
10	83.1	3.1	506.4
10	63.7	4.1	506.0
10	57.6	4.5	505.8
10	33.4	7.8	504.1

TABLE 10. STEADY-STATE REACTOR TEMPERATURES WITH POWER OF 74 MEGAWATTS AND FULL FLOW OF 8×10^6 LB PER HR

Second Pass	Temperature, F	Third Pass	Temperature, F
θ_{2_1}	732	θ_{3_1}	1202
θ_{2_2}	720	θ_{3_2}	1156
θ_{2_3}	695	θ_{3_3}	1067
θ_{2_4}	658	θ_{3_4}	943
θ_{2_5}	613	θ_{3_5}	796
θ_{He_2}	550	θ_{He_3}	636
θ_{s_2}	514	θ_{s_3}	542
θ_{f_2}	660	θ_{f_3}	952
$\theta_{c_{bc}}$	499	$\theta_{c_{de}}$	512
T_{c_b}	495	T_{c_d}	502
T_{c_c}	502	T_{c_e}	521

TABLE 11. REACTOR TEMPERATURE COEFFICIENTS

Coefficient	Symbol	Associated Temperature	Value, δk per F
Moderator coefficient			
Second pass	α_2	$\theta_{c_{bc}}$	-0.28×10^{-4} -0.52×10^{-4}(a) -0.59×10^{-4}
Third pass	α_3	$\theta_{c_{de}}$	-1.20×10^{-4} -2.25×10^{-4}(a) -2.51×10^{-4}
Doppler coefficient	α_d	$\bar{\theta}_f$	-1.0×10^{-5} -2.3×10^{-5}(a) -5.0×10^{-5}

(a) Standard value.

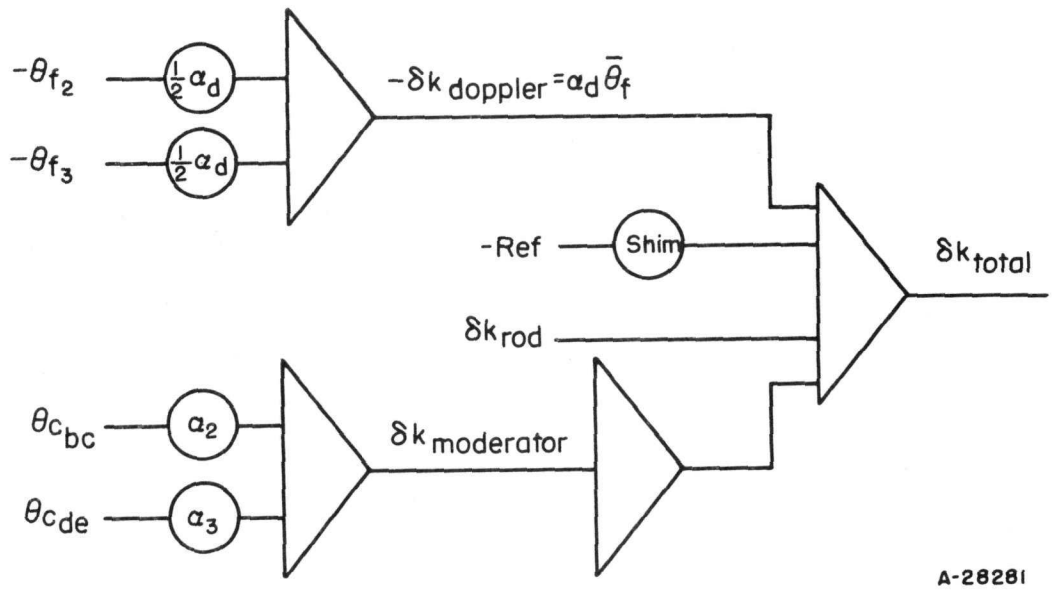

FIGURE 10. REACTIVITY SIMULATION

Therefore, the reactivity equation becomes:

$$\delta k_{total} = \delta k_{shim} + \delta k_{rod} + \alpha_2 \theta_{c_{bc}} + \alpha_3 \theta_{c_{de}} + \alpha_d \bar{\theta}_f \ . \qquad (29)$$

The function δk_{rod} will be discussed with the individual accidents.

The purpose of δk_{shim} is to establish the initial power levels from which the accidents begin.

Reactor Period

The reactor period has been defined as the amount of time it takes for the neutron flux to change by a factor e. In simulation studies of power reactors, the flux ϕ and power level P_r are considered interchangeable.

If T is the reactor period, then

$$\phi = \phi_o e^{t/T} , \tag{30}$$

or

$$1/T = (1/P_r) \frac{d}{dt} P_r . \tag{31}$$

However, the kinetic equations have been solved directly for P_r; thus, to obtain $1/T$ by use of Equation (30), the power signal would have to be differentiated. Since electronic differentiation is a noise-amplifying process, care must be taken to generate a period signal. The P_r output signal from the feedback unit also has noisy characteristics, and a straightforward simulation involving a servo-dividing circuit would only complicate the situation.

In actual reactor period circuits the approach is to obtain the natural logarithm of power and then differentiate:

$$\frac{d}{dt} \log_e P_r = (1/P_r) \frac{d}{dt} P_r . \tag{32}$$

Thus, a simulation circuit was devised to express $\log_e P_r$. Figure 11 shows the simulation used to represent the reciprocal period. The log circuit output is $A \log_e P_r + C$. This circuit was checked with a P_r input function to verify that the log and period circuits were functioning properly. The proportionality constant A for this configuration was found to be 0.086. The 400-kilohm resistor in the period circuit represents a time constant of 400 milliseconds, the standard value used in these studies.

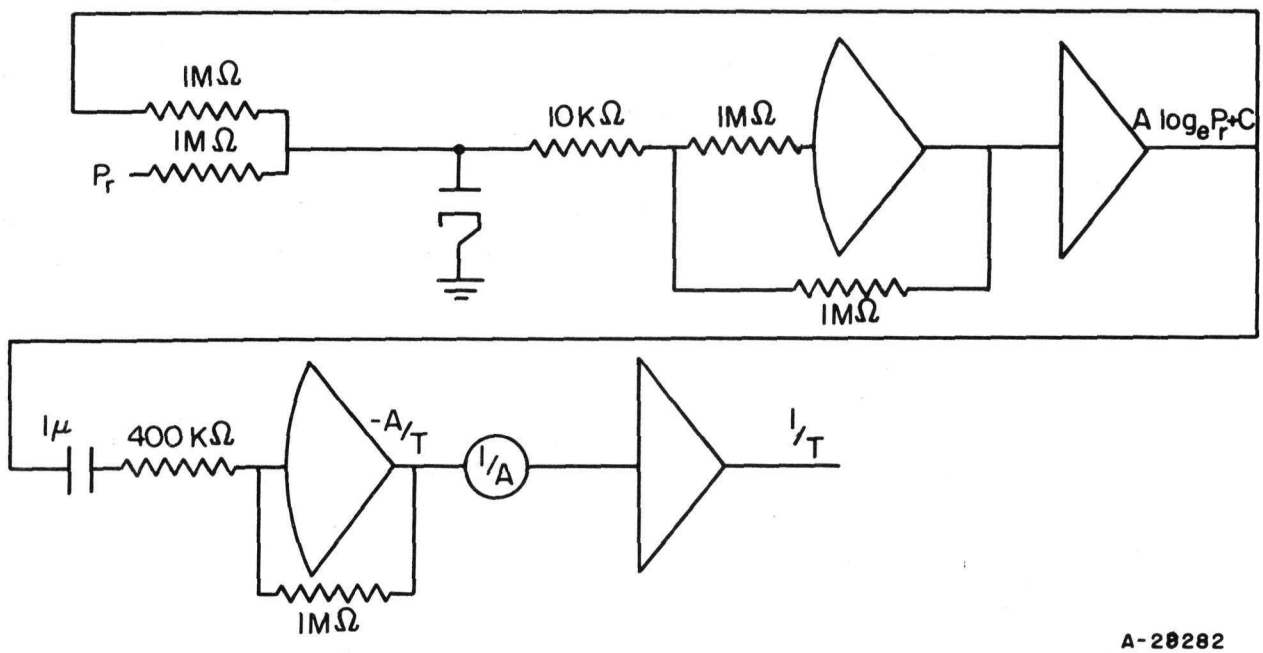

FIGURE 11. RECIPROCAL PERIOD SIMULATION

CONTINUOUS-ROD-WITHDRAWAL ACCIDENT

The continuous-rod-withdrawal accident was simulated under the following conditions. With the reactor critical and operating at various initial power levels and flow rates, the bank of control rods which contains the maximum reactivity worth was withdrawn at the maximum possible velocity. This could occur due to a malfunction at the control system.

The investigation involved three phases: (1) no safety system in operation, (2) period trip, and (3) high-flux trip.

In the first phase, the rods were allowed to continue their withdrawal until the cladding temperature in the third phase reached 620 F. The saturation steam temperature at 1750 psi is about 620 F. At this temperature boiling would occur, creating steam voids in the system. The effect of these voids is to cut down the reactivity and thus to decrease the rate of power increase. The runs were incorrect after boiling occurred because of a breakdown in the simulation of the system under this condition.

Scramming of the reactor would be initiated by one of two criteria, high flux or short period. Using the high-flux trip, the system was examined to determine what increase in system temperature occurs before scram, and also the characteristics of the reactor response to scram.

Rod-Withdrawal Simulation

The investigation of this accident was accomplished with a simulation of the reactor alone, as described in the previous sections.

The portion of the simulation peculiar to this accident involves only a representation of the reactivity ramp function and provision for a scram function to be injected into the total δk. The rate of rod withdrawal was integrated with respect to time and fed into the δk_{total} simulation. For no safety system, this was all that was required. For flux and period scrams, relay networks were used to cut off the rod withdrawal and insert the δk scram function. This scram function was produced by a diode function generator. The minimum-scram curve, standard condition, showing negative reactivity versus time is shown in Figure 12.

Additional relay networks were used to short out the disturbance after scram so that the computer could operate continuously and not have to be reset after each run. Another circuit was used to mark the beginning of rod withdrawal and time of scram on the output data.

Since the primary-coolant loop and boiler were not considered in this simulation, the assumption had to be made that the inlet coolant temperature, T_{c_b}, was constant at the values listed previously in Table 9. This assumption was considered to be conservative since the inlet temperature would increase with rod withdrawal, causing a general increase in all system temperatures. These increased temperatures would reduce the power excursion due to the negative temperature coefficients of reactivity.

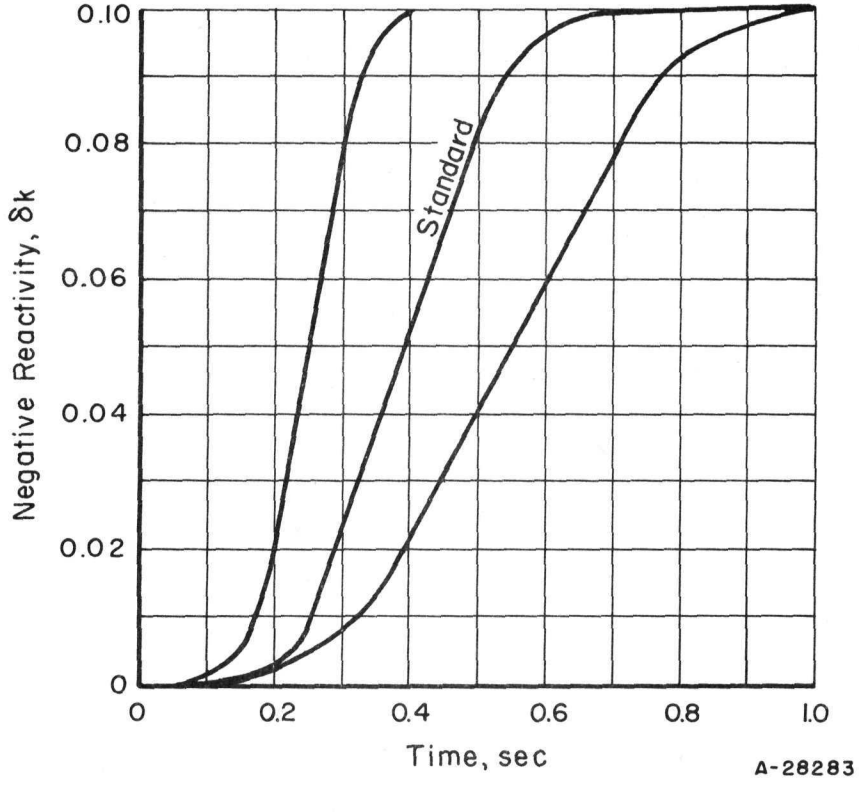

FIGURE 12. SCRAM CURVES

Program Analysis and Discussion for Rod-Withdrawal Accident

The analysis of this accident included variation of the following parameters:

(1) Power level

(2) Flow rate

(3) Rate of reactivity insertion

(4) Period for scram

(5) Delay in period circuitry

(6) Flux scram level

(7) Scram delay time

(8) Minimum scram function of negative reactivity versus time

(9) Moderator-temperature coefficient

(10) Doppler coefficient

(11) Total negative reactivity available for shutdown.

Table 12 lists the values of these parameters not already reported.

Figure 13 shows the response of the system, initially at 100 per cent power and 100 per cent flow, with all other parameters at their estimated design values, with no safety system in operation. The response of the reactor, scrammed at 100 megawatts, 135 per cent of rated power, is shown in Figure 14.

Table 13 shows the comparison of operation with no safety system at the time the cladding in the third pass reaches 620 F and high-flux-trip operation.

Rod-Withdrawal-Investigation Results

Results of the "no safety system in operation" phase indicate that, with the inherent stability of the reactor (i. e. , the existence of high negative temperature coefficients of reactivity), the period never decreases below 16 sec. Consequently, the study of the response to period trip was unnecessary. In addition, it was found that variations in scram delay time and scram rate produced little effect because of the rapid response of the system to scram. The same is true for variations in Doppler and moderator coefficients, and high-flux-trip levels.

At low power levels, the time elapse before scram was longer, but the excursions were about the same. At low flow rates, the excursions were less than under standard operating conditions. The results shown in Figures 13 and 14 are representative of the

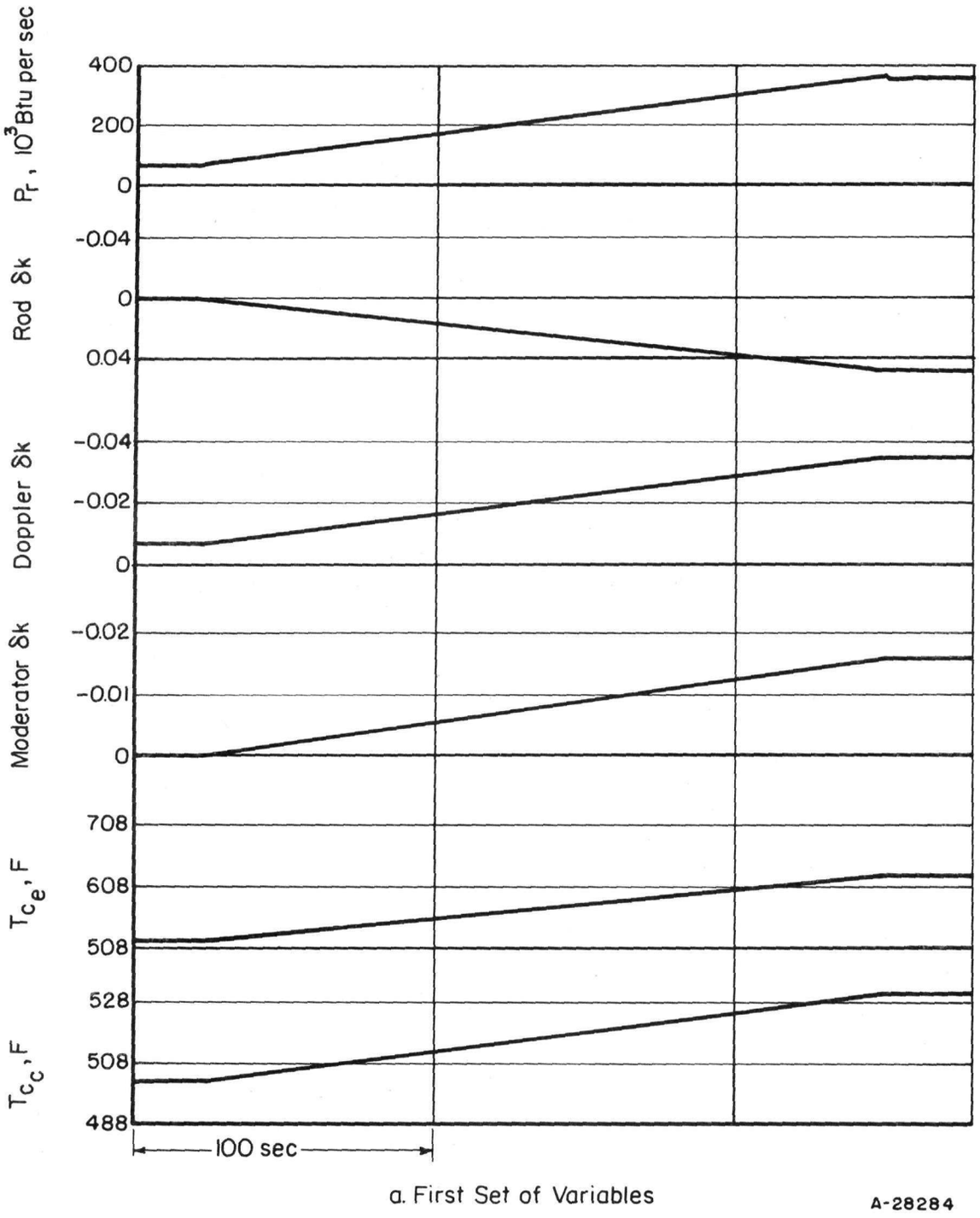

a. First Set of Variables

FIGURE 13. RESPONSE OF SYSTEM AT 100 PER CENT POWER AND 100 PER CENT FLOW TO CONTINUOUS ROD WITHDRAWAL WITH NO SAFETY SYSTEM IN OPERATION

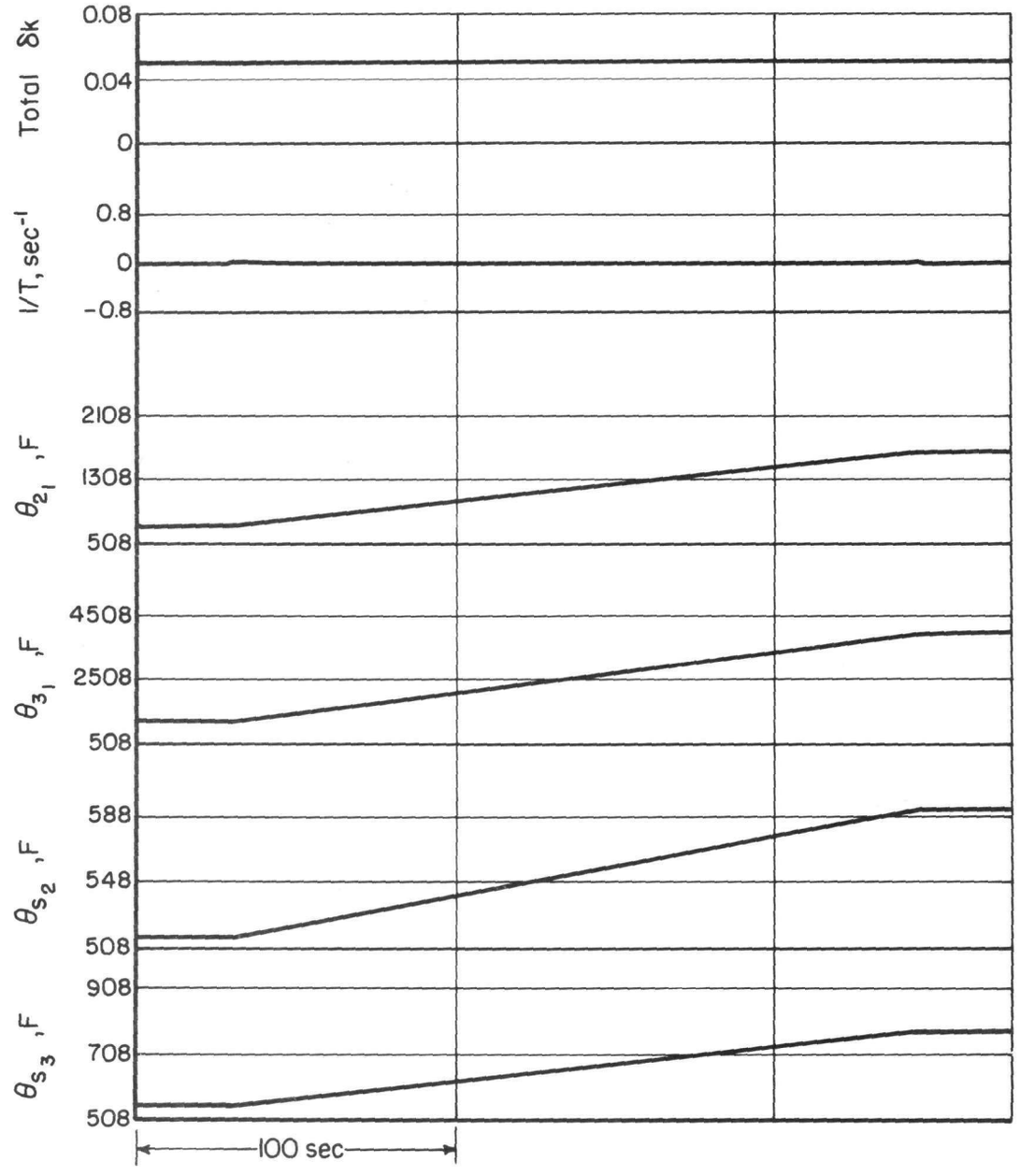

b. Second Set of Variables

FIGURE 13. (CONTINUED)

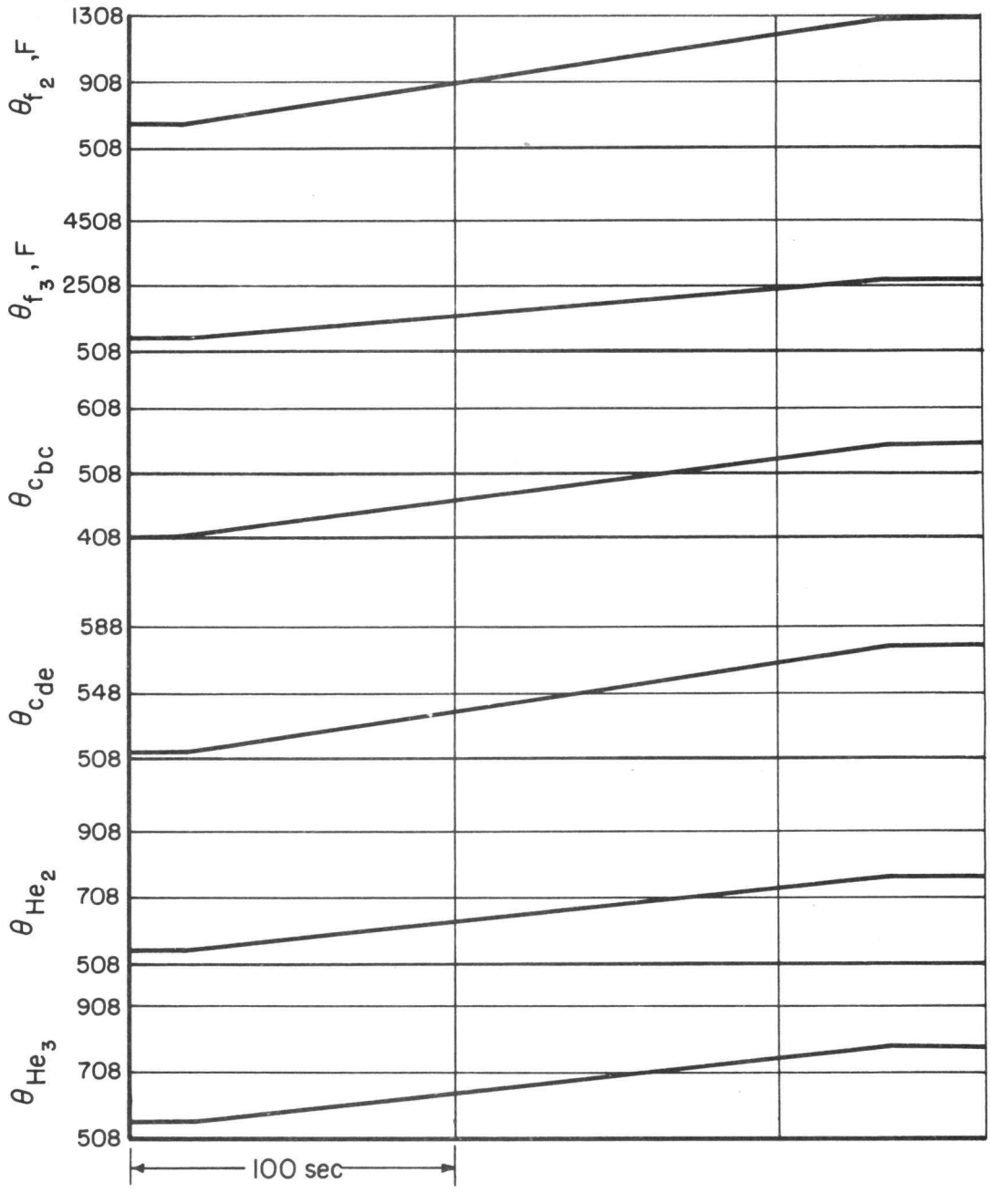

c. Third Set of Variables

FIGURE 13. (CONTINUED)

TABLE 12. PARAMETERS OF CONTINUOUS-ROD-WITHDRAWAL ACCIDENT

Rate of Reactivity Insertion, δk per sec	4×10^{-4}
	2×10^{-4}(a)
	1×10^{-4}
	5×10^{-5}
Period for Scram, sec	10
	1(a)
	0.1
Delay in Period Circuitry, milliseconds	110
	200
	400(a)
	600
	1100
Flux Scram Level at Indicated Percentage of Full Flow, megawatts	
100	81
	100(a)
	122
83.1	67
	85(a)
	100
63.7	50
	62(a)
	74
57.6	44
	55(a)
	66
33.4	22
	28(a)
	33
Scram Delay Time, milliseconds	100
	240(a)
	400
Total Negative Reactivity Available for Shutdown, δk	0.01
	0.03(a)
	0.10

(a) Estimated design value.

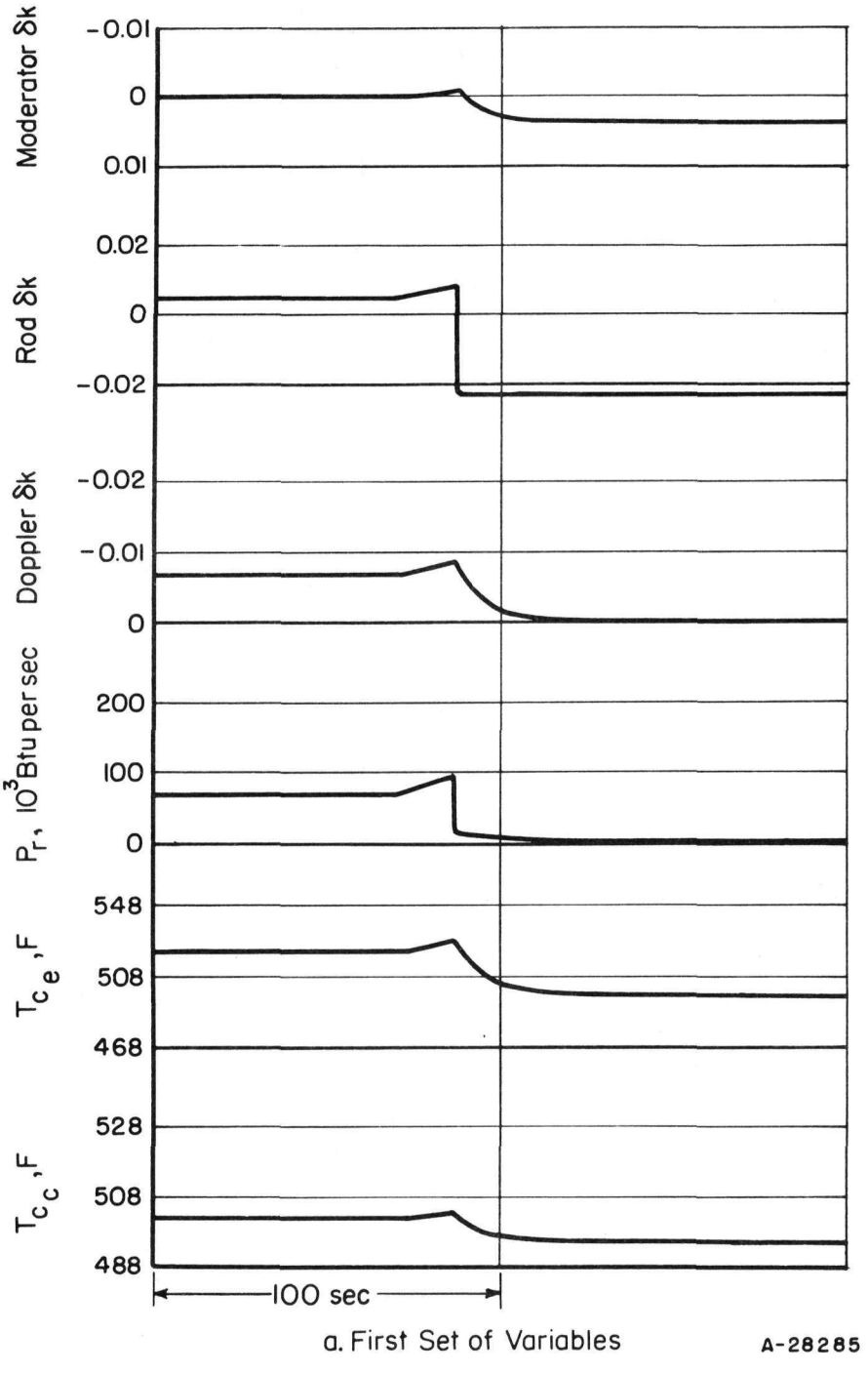

FIGURE 14. RESPONSE OF SYSTEM AT 100 PER CENT POWER AND 100 PER CENT FLOW TO CONTINUOUS ROD WITHDRAWAL WITH SCRAM AT 100 MEGAWATTS

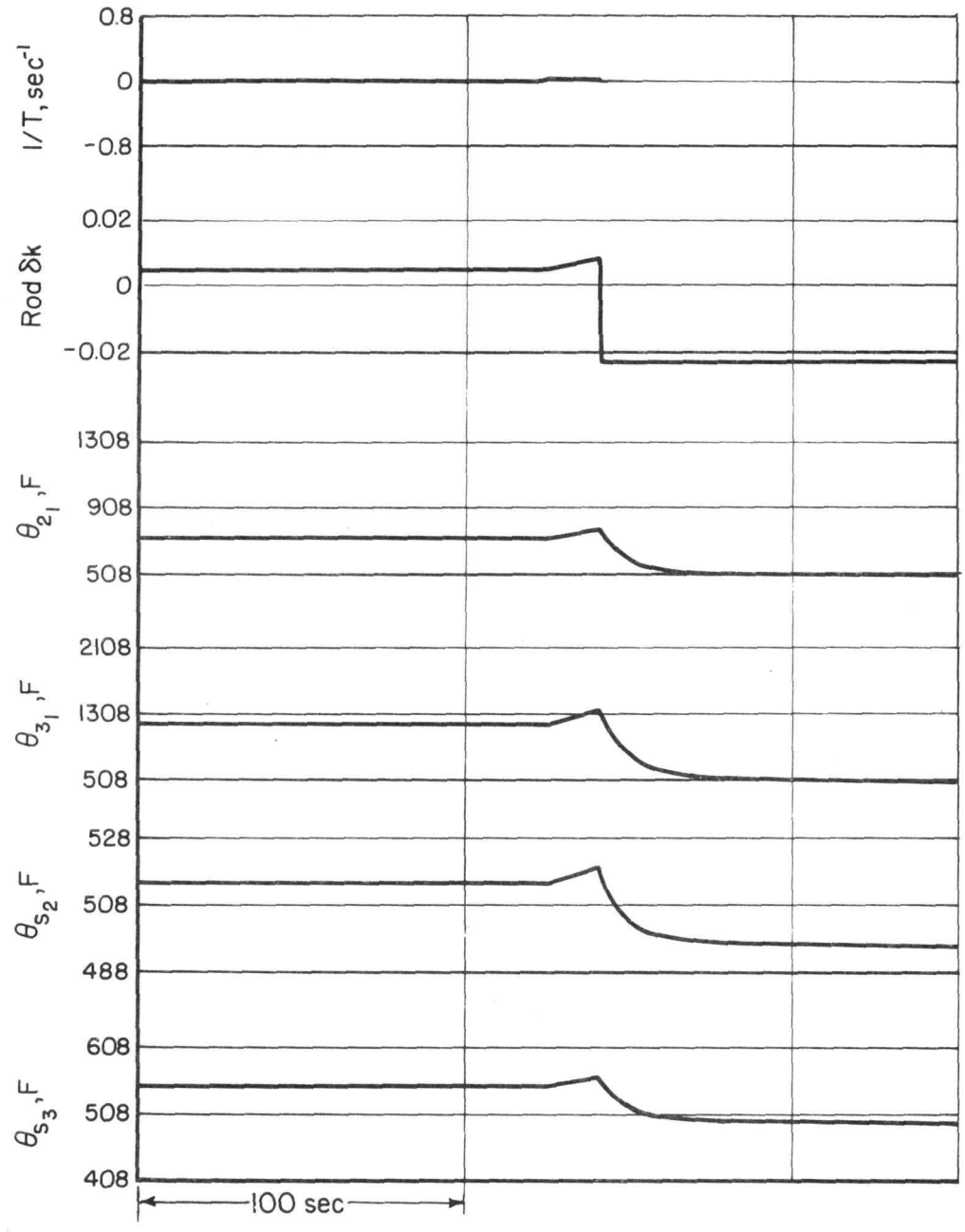

b. Second Set of Variables

FIGURE 14. (CONTINUED)

TABLE 13. COMPARISON OF SYSTEM TEMPERATURES, WITH AND WITHOUT FLUX SCRAM

	Initial Condition	No Scram System	High-Flux Scram
Flow, per cent	100		
Power, megawatts	74.0	158	100
Time, sec		60	17.5
Temperature, F			
θ_{3_1}	1202	1900	1348
θ_{s_3}	552	620	563
T_{c_e}	521	546	527
Flow, per cent	83.1		
Power, megawatts	60.7	144	85
Time, sec		73	18.0
Temperature, F			
θ_{3_1}	1028	1870	1228
θ_{s_3}	543	620	563
T_{c_e}	523	560	531
Flow, per cent	63.7		
Power, megawatts	45.1	101	62
Time, sec		58	14.5
Temperature, F			
θ_{3_1}	948	1430	1048
θ_{s_3}	548	620	561
T_{c_e}	529	565	536
Flow, per cent	57.6		
Power, megawatts	40.0	89.5	55
Time, sec		60	14.5
Temperature, F			
θ_{3_1}	898	1350	988
θ_{s_3}	548	620	559
T_{c_e}	529	570	537
Flow, per cent	33.4		
Power, megawatts	20.0	52.5	28
Time, sec		65	12.5
Temperature, F			
θ_{3_1}	708	1025	748
θ_{s_3}	544	620	553
T_{c_e}	539	610	547

system response to conditions of continuous rod withdrawal with any combination of system parameters.

Figure 14 reveals that, following scram, the reactor power drops almost immediately to a particular low level dependent upon the total negative reactivity used for shutdown.

STARTUP ACCIDENT

The objectives of startup are to bring the cold reactor to critical and then to increase the power level in a controlled manner until desired power is reached. This is done by withdrawal of control rods. In a reactor designed for high power levels, these rods must be withdrawn fairly rapidly until criticality is approached to minimize the time required for startup. If, as a result of some malfunction, this rapid withdrawal is continued through the prompt-critical stage, the power will rapidly exceed the normal operating level. It is important from a safety standpoint to determine the extent of power and temperature excursions in the event of such an accident.

The power and temperature excursions were determined from an analog simulation of the reactor system. This simulation of the reactor from a cold subcritical condition to a prompt-critical reactor was performed in three steps. First, a linear simulation was carried out for the change in reactivity from subcritical to critical and an increase in power level by approximately one decade. Second, an exponential simulation was used for an increase in reactor power by a factor of approximately 10^9. During this time the simulated reactor was entering the prompt-critical stage. Third, a linear simulation was employed to study the system in the operating-power range.

Startup Simulation

During the first and second phases, the total energy produced by the reactor is not large enough to result in a measurable rise in temperature in the reactor. Therefore, the fuel-pin- and coolant-temperature simulations were omitted.

Subcritical Linear Simulation

The reactor kinetics were represented by Equations (1) through (7). For this study these equations were simulated using standard analog computing techniques so that computation could be stopped, and final values of power and the concentration of the delayed-neutron groups could be determined. The computer diagram for this system is shown in Figure 15.

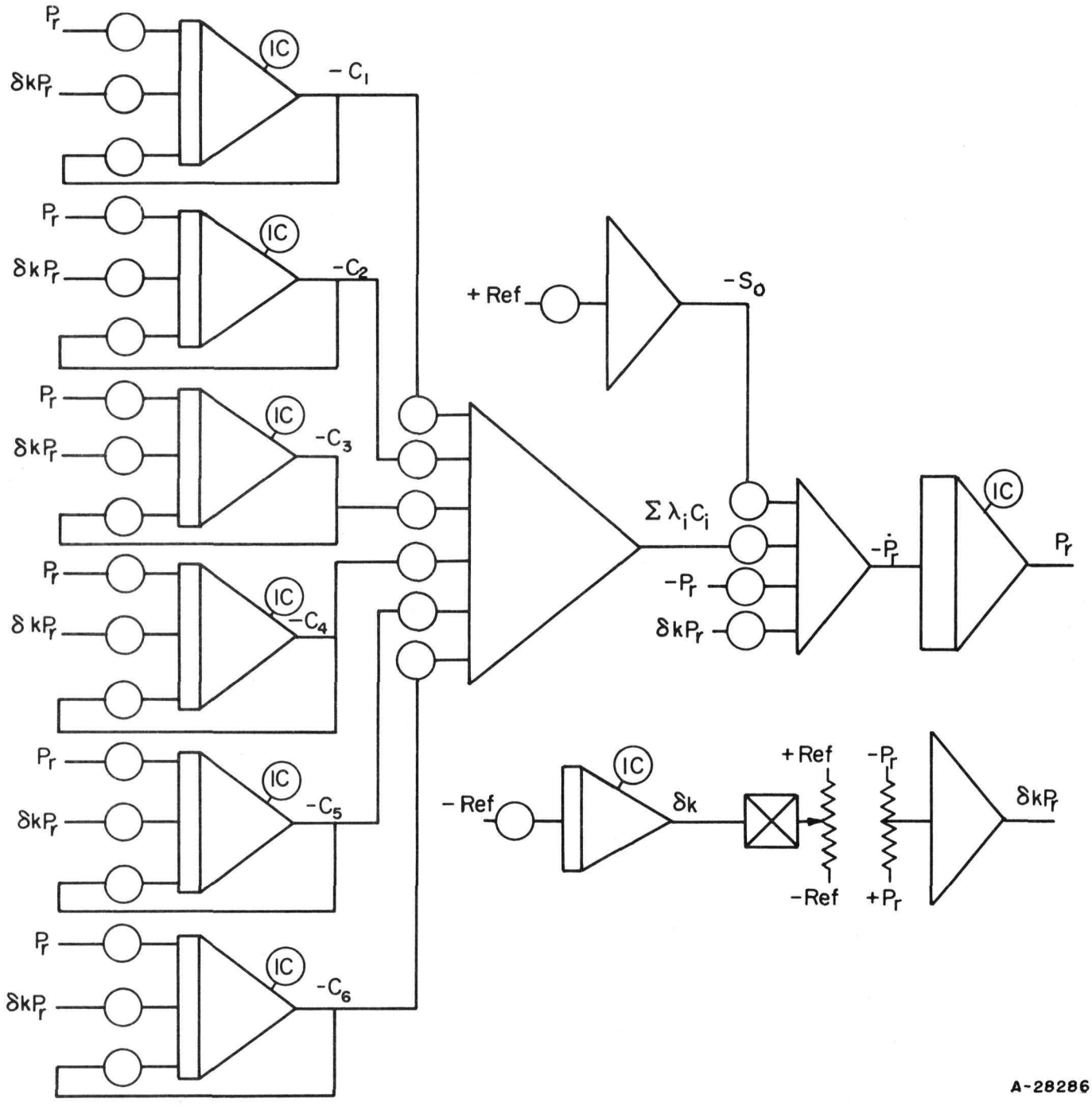

FIGURE 15. LINEAR REACTOR COMPUTER DIAGRAM FOR STARTUP ACCIDENT

Critical Exponential Simulation

Because of the large range of power involved in this phase of the study, a factor of approximately 10^9, a standard linear simulation would not be satisfactory. In order to obtain variables which change by less than 10^2, the following substitutions were made in Equations (1) through (7):

$$P_r' = P_r e^{-xt^2}, \tag{33}$$

$$C_i' = C_i e^{-xt^2}, \tag{34}$$

where x is an arbitrary constant chosen to allow a convenient change in P_r'. Differentiation of Equations (33) and (34) gives:

$$\dot{P}_r' = \dot{P}_r e^{-xt^2} - 2xt\ P_r e^{-xt^2}, \tag{35}$$

$$\dot{C}_i' = \dot{C}_i e^{-xt^2} - 2xt\ C_i e^{-xt^2}. \tag{36}$$

Substituting Equations (33) through (36) into Equations (1) through (7) and simplifying gives:

$$P_r' = \left[\frac{(1 - B)k - 1}{\ell} - 2xt \right] P_r' + \sum \lambda_i C_i' + S_o e^{-xt^2}, \tag{37}$$

$$\dot{C}_i' = -(\lambda_i + 2xt)\ C_i' + \frac{\beta_i k}{\ell} P_r'. \tag{38-43}$$

The computer diagram for the reactor-kinetics portion of this system is shown in Figure 16. The initial conditions for this phase were taken from the final conditions of the first-phase runs.

Power-Level Linear Simulation

The reactor kinetics for this phase were simulated as in the subcritical linear phase. This simulation was coupled to the fuel-pin simulation as previously described. This phase was run at 1/100 real time. The initial conditions for this phase were taken from the final conditions of the second-phase runs.

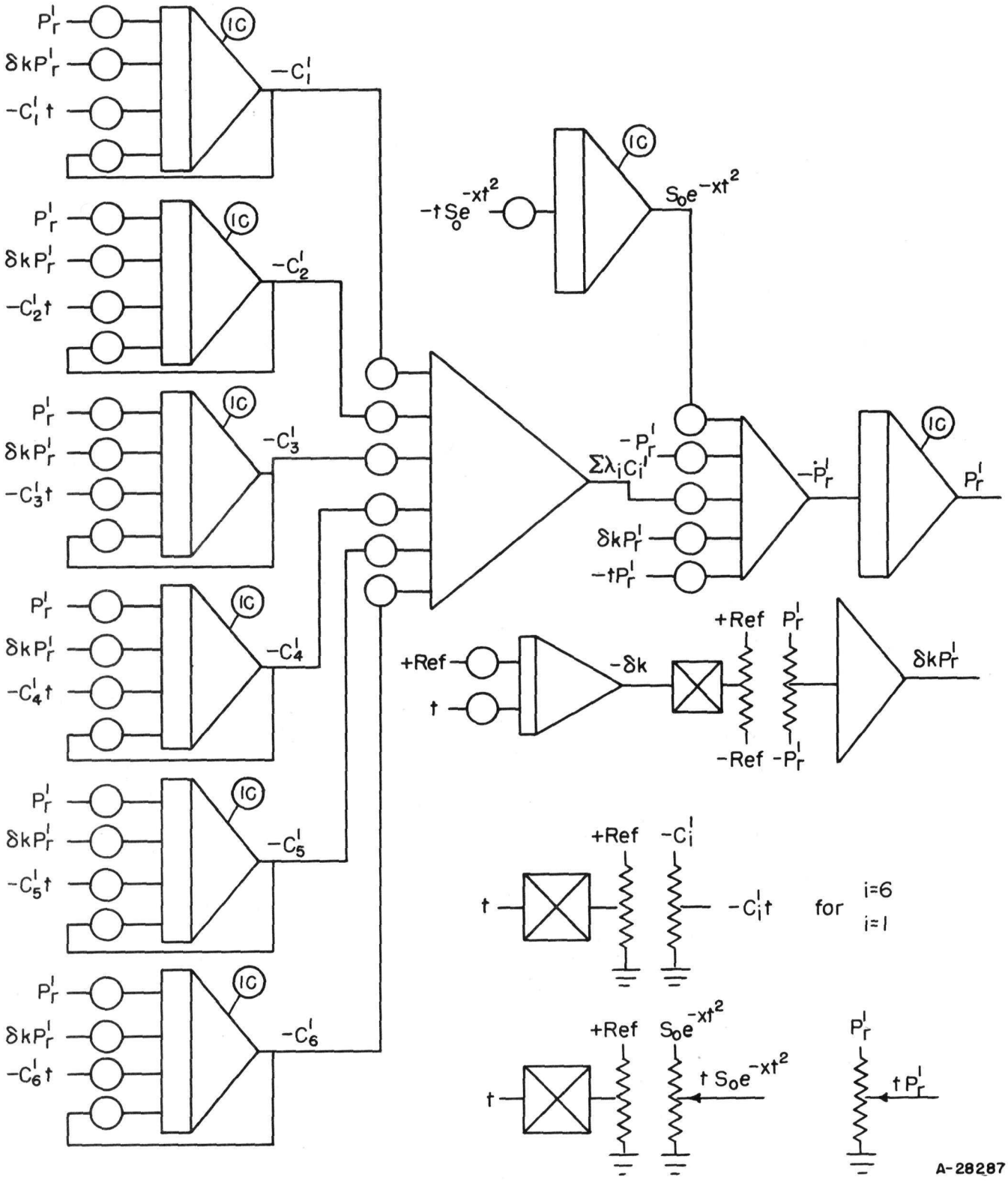

FIGURE 16. COMPUTER DIAGRAM FOR EXPONENTIAL SIMULATION OF REACTOR

Program Analysis and Discussion for Startup Accident

During the first and second phases, the only parameters to be varied were initial subcriticality and rod-withdrawal rate. Initial subcriticalities varied from 1 to 15 per cent. Two rod-withdrawal rates were used, 1×10^{-3} and 3×10^{-4} δk per sec. Variations in these parameters made only minor changes in the period of the reactor when the operating-power level was reached.

During the third phase the effects of the following parameters were examined: temperature coefficient of reactivity, Doppler coefficient, high-flux-trip level, scram delay time, reactivity available for shutdown and scram insertion rate, as well as initial subcriticality and rod-withdrawal rate.

The results of the startup accident using standard values of parameters with no safety system are shown in Figure 17. Figure 18 shows the results of the same system with high-flux scram.

Startup Investigation Results

The only parameters which appreciably affected the power excursion during this accident were the Doppler coefficient and the rod-withdrawal rate. The high Doppler coefficient produced more negative reactivity for the same increase in fuel-pin temperature, and, therefore, limited the power excursion sooner and at a lower value. The low withdrawal rate produced a slower change in excess reactivity and therefore permitted more time for the fuel pins to heat and stop the power rise through the action of the Doppler coefficient. However, even with the worst power excursions, the temperatures in the system remained below operating level temperatures.

Figure 19 is a plot of the reactor power level versus time for complete accident from initial subcriticality through the power peak and the final decrease due to the effect of the Doppler coefficient.

LOSS-OF-COOLANT-FLOW ACCIDENT

In this study the response of the reactor to the simultaneous failure, due to loss of power, of all operating coolant pumps was investigated. The rapid decrease in coolant flow results in an inability of the coolant to remove all the heat generated by the reactor. Therefore, the system temperatures increase. As the heat-transfer coefficient decreases, the fuel temperatures increase further.

Even neglecting the effect of steam-void formation, the negative temperature coefficients of reactivity are sufficient to lower the power level in a relatively short time. However, the temperature rise may be excessive and scramming would be necessary to prevent physical damage to the reactor, such as melting of the fuel pins.

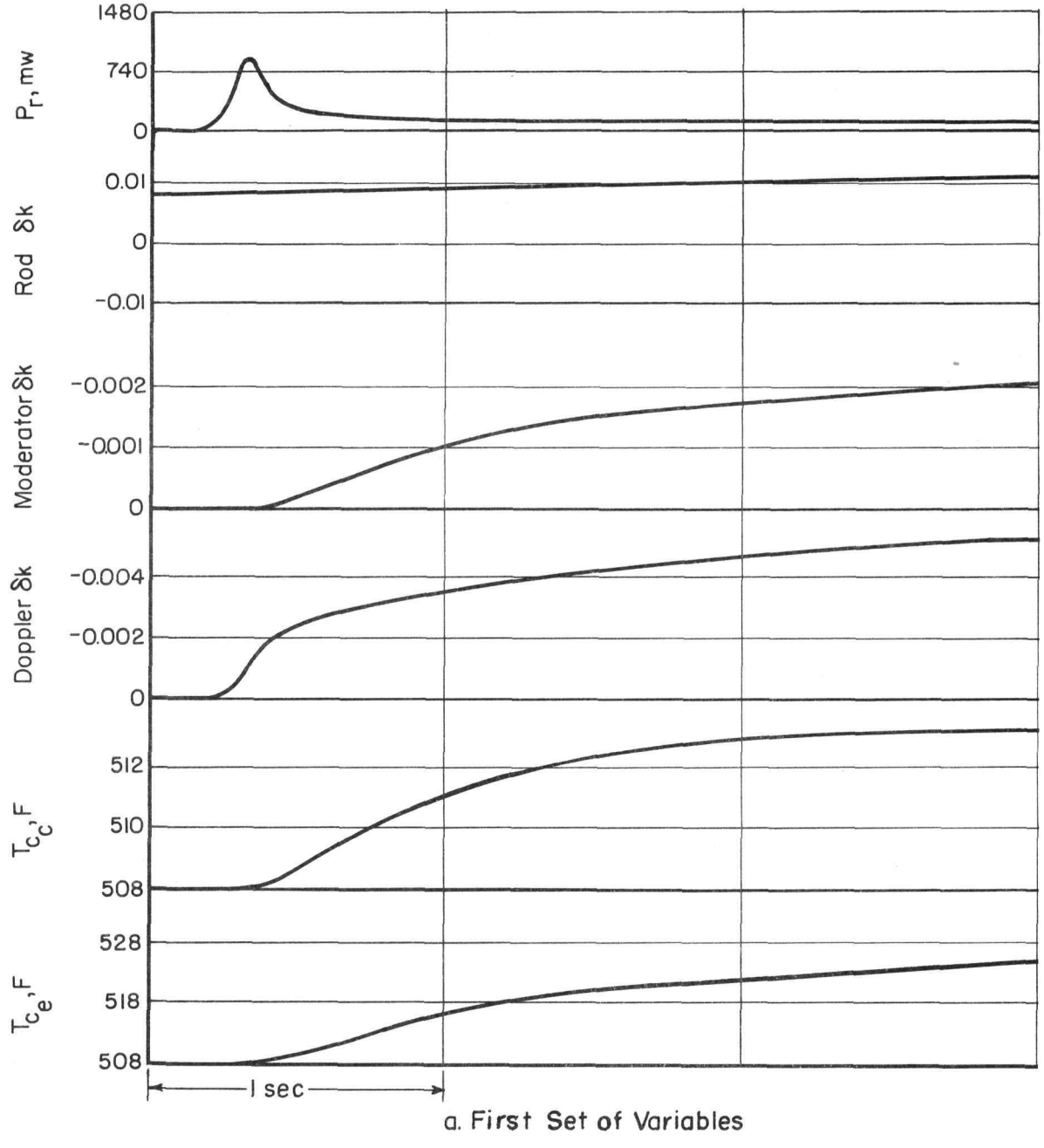

FIGURE 17. RESPONSE OF SYSTEM FROM 5 PER CENT POWER TO STARTUP WITH NO SAFETY SYSTEM IN OPERATION

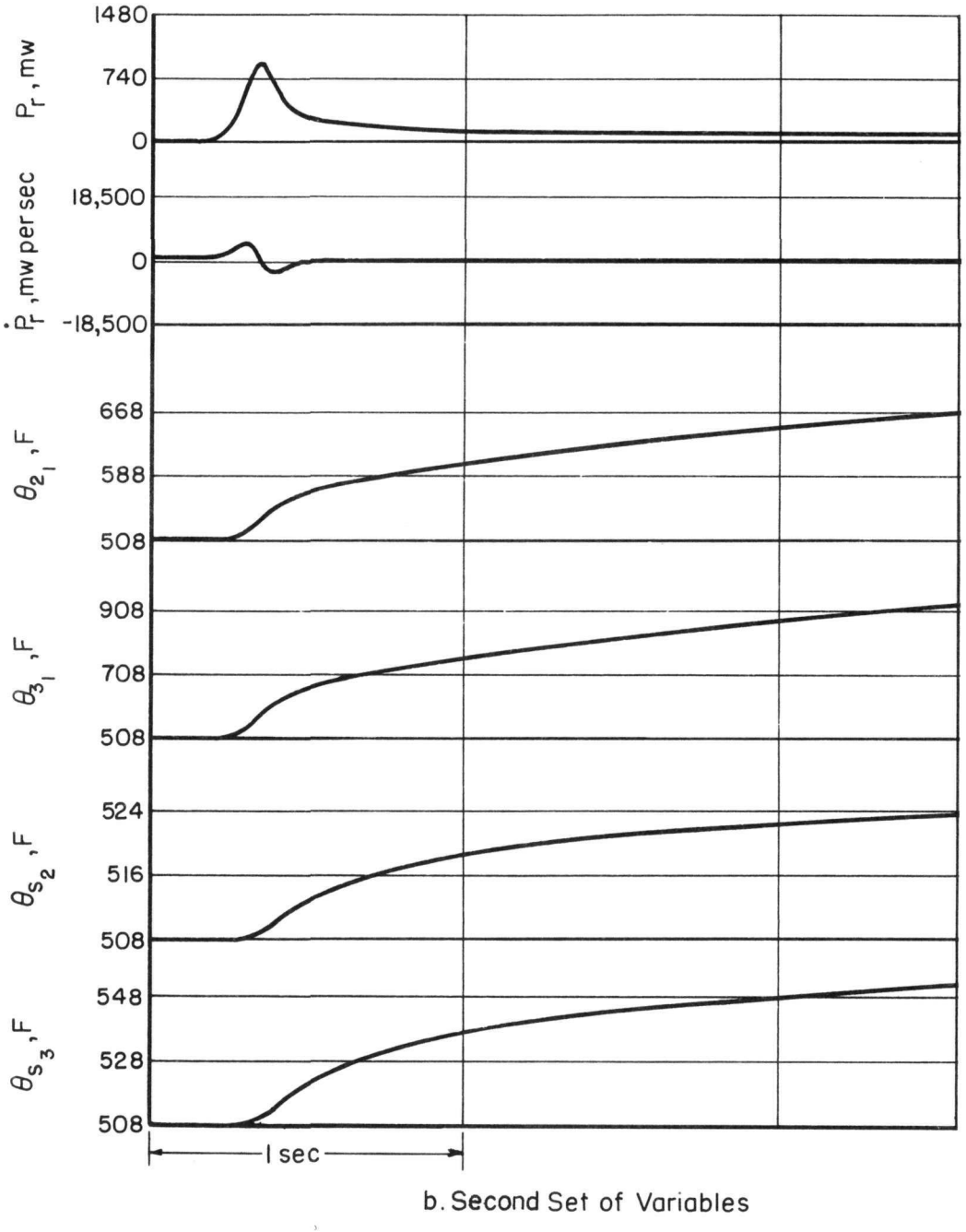

FIGURE 17. (CONTINUED)

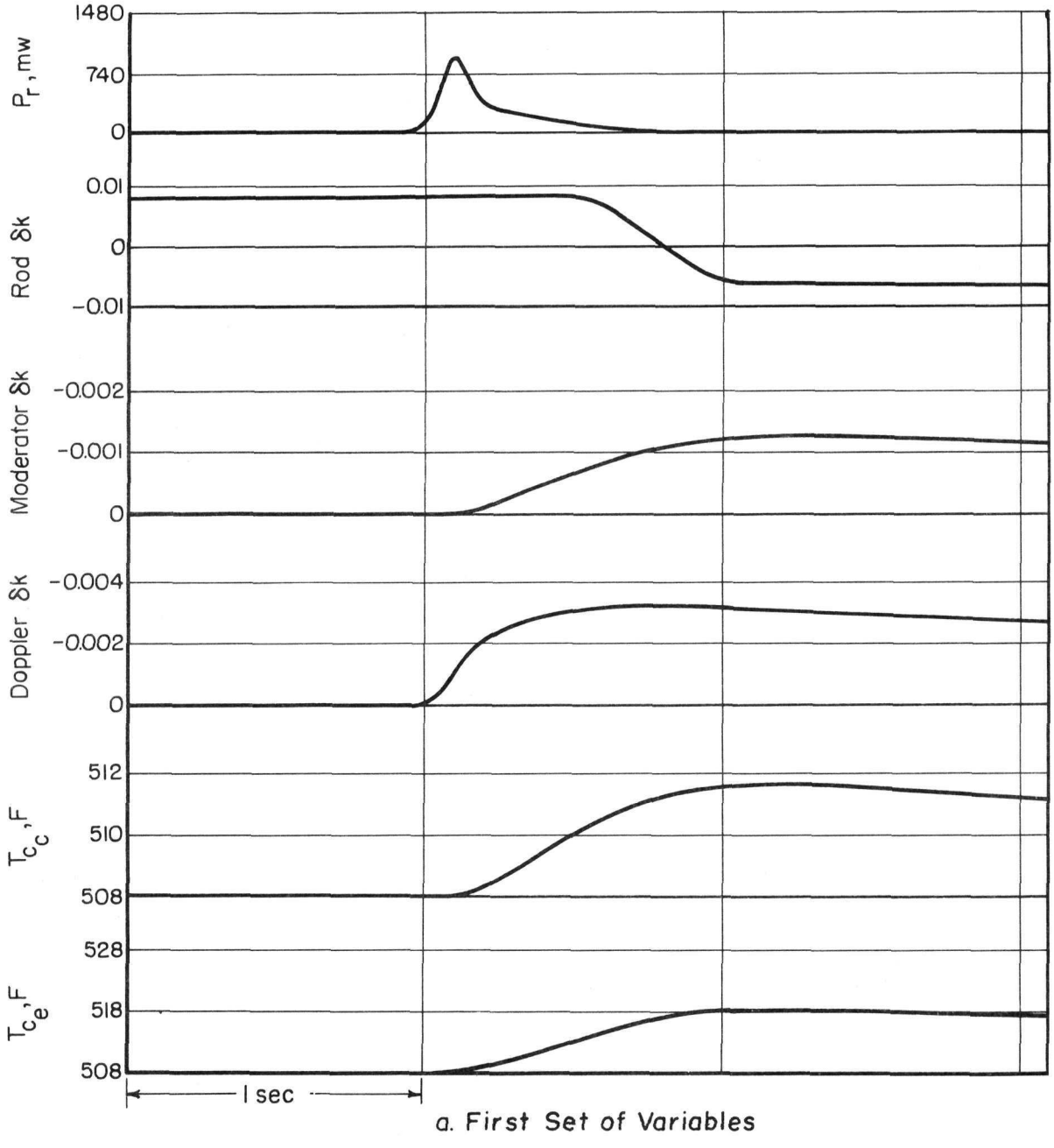

FIGURE 18. RESPONSE OF SYSTEM FROM 5 PER CENT POWER TO STARTUP WITH SCRAM AT 100 MEGAWATTS

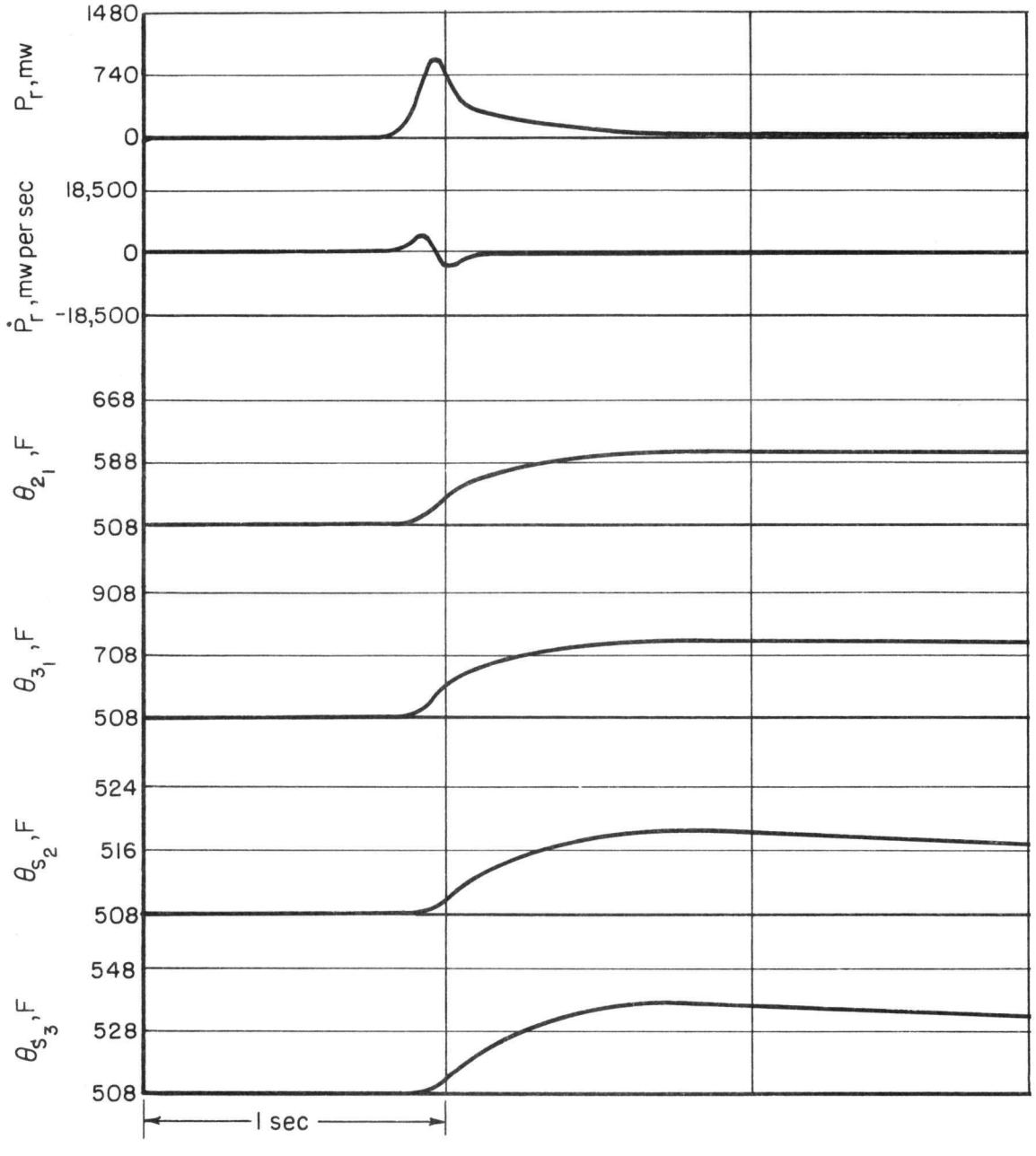

b. Second Set of Variables

A-28289

FIGURE 18. (CONTINUED)

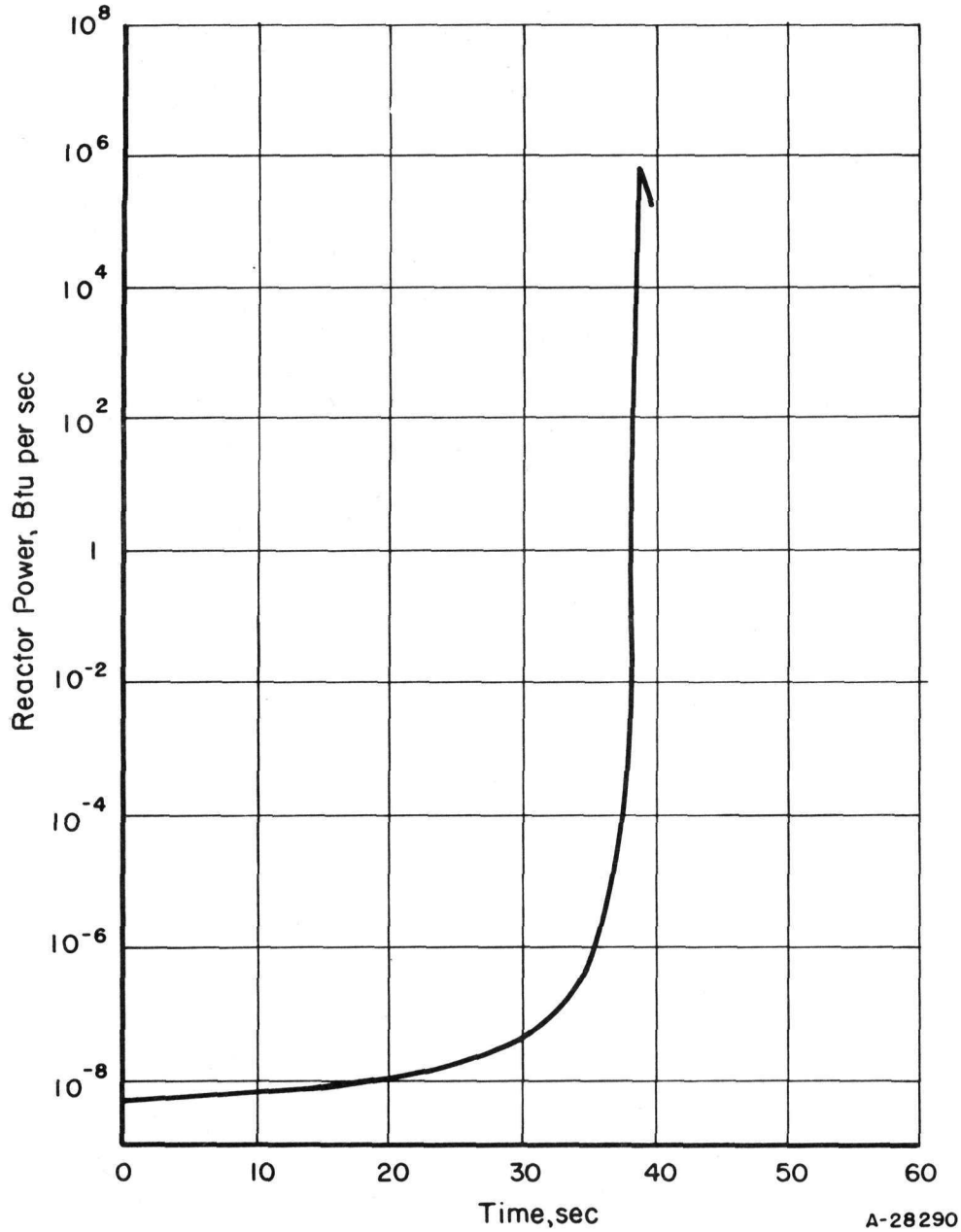

FIGURE 19. REACTOR POWER FOR STARTUP WITH 3 PER CENT SUBCRITICALITY AND STANDARD ROD-WITHDRAWAL RATE

Transient flow data for this reactor system for accidents involving the loss of forced coolant flow and cold-water insertion were supplied by The Babcock & Wilcox Company, Atomic Energy Division. Two cases of coastdown were considered:

(1) Four pumps at full speed coasting to no pumps

(2) Two pumps, one per loop, at one-half speed, coasting to no pumps.

The first case represents the extreme accident under normal operating conditions; the second, the conditions of loss of flow during low power operation.

Two variable input functions were involved in this analysis. The flow function, W(t), was integrated. The resulting curve was used to obtain the transport delays in the second and third passes. The heat-transfer coefficient between the steel and coolant, h(t), was obtained by applying Equation (24). The coastdown curves for the two cases considered are shown in Figures 20 and 21.

The purpose of this study was to investigate the system response to coastdown, with and without scram, and to optimize the scram parameters for safe shutdown.

Loss-of-Flow Simulation

The simulation can be modified for this accident by eliminating the turnaround (3.007-sec delay), since coolant leaving the second pass will not reach the third pass before flow stops. Therefore the inlet temperature to the second and third passes was assumed to be constant.

The coolant-film coefficient, k_d, was replaced by h(t) in the pin simulation. This and the variable time delay, τ, were incorporated into the reactor coolant temperature simulation as shown in Figure 22. To simplify notation G(t) is defined as:

$$G(t) = \frac{k_c\, h(t)}{\Delta r_c k_c + h(t)\,\frac{\Delta r_c^2}{2}} \cdot \frac{1}{c_c \rho_c} \qquad (44)$$

This was simulated by use of diode function generators. The heat-transfer film coefficient as function of time is shown in Figure 23. Since the relation of Equation (24) is not strictly valid for low flow rates, it was assumed that after 6 sec of coastdown, h(t) goes to zero. At this point the simulation becomes that of an insulated fuel pin.

Since the transport time was defined as the length of time for a particle at the inlet to reach the outlet, the initial delay becomes 0.976 sec through the second pass and 1.09 sec through the third pass. The variation of the delays with time are shown in Figure 24. Table 14 relates the initial system temperatures for the four-pump case consistent with these increased delay times.

For the two-pump case, the initial power level was 17.8 megawatts, and the flow was 31.6 per cent of full flow. During flow coastdown, the transport lag time increased so rapidly that an assumption that the flow would immediately drop to zero is a good

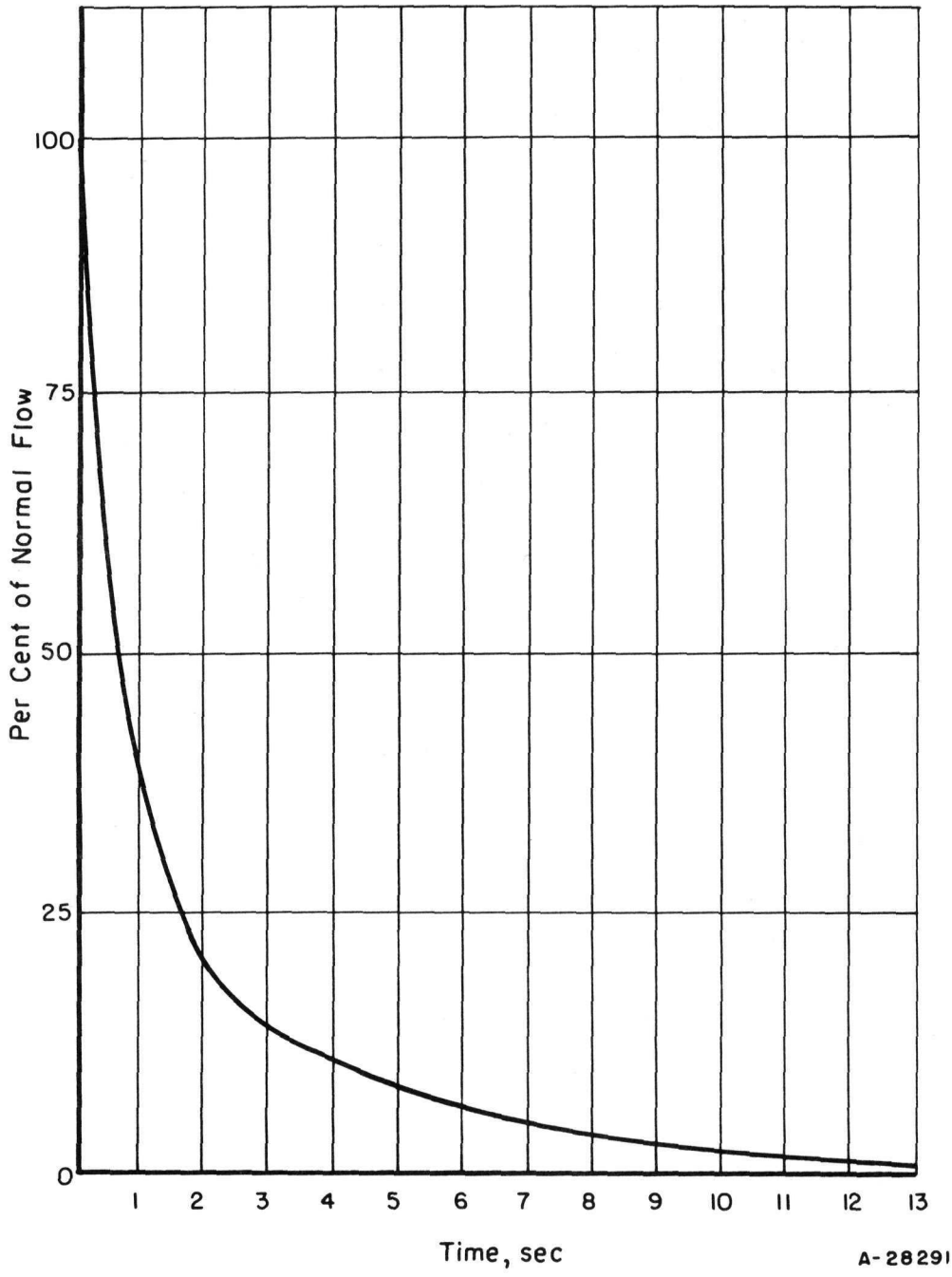

FIGURE 20. TOTAL COASTDOWN FROM FOUR PUMPS AT FULL SPEED

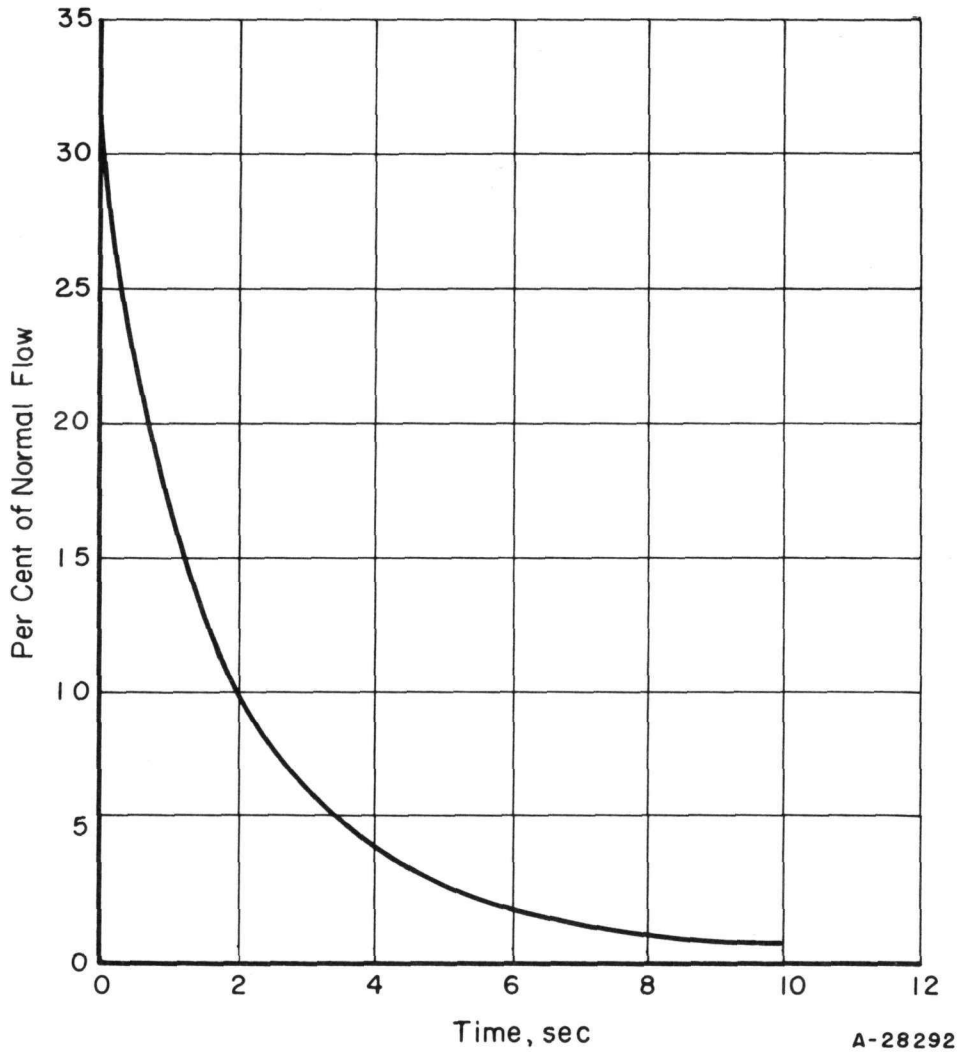

FIGURE 21. TOTAL COASTDOWN FROM TWO PUMPS, ONE PER LOOP, AT HALF SPEED

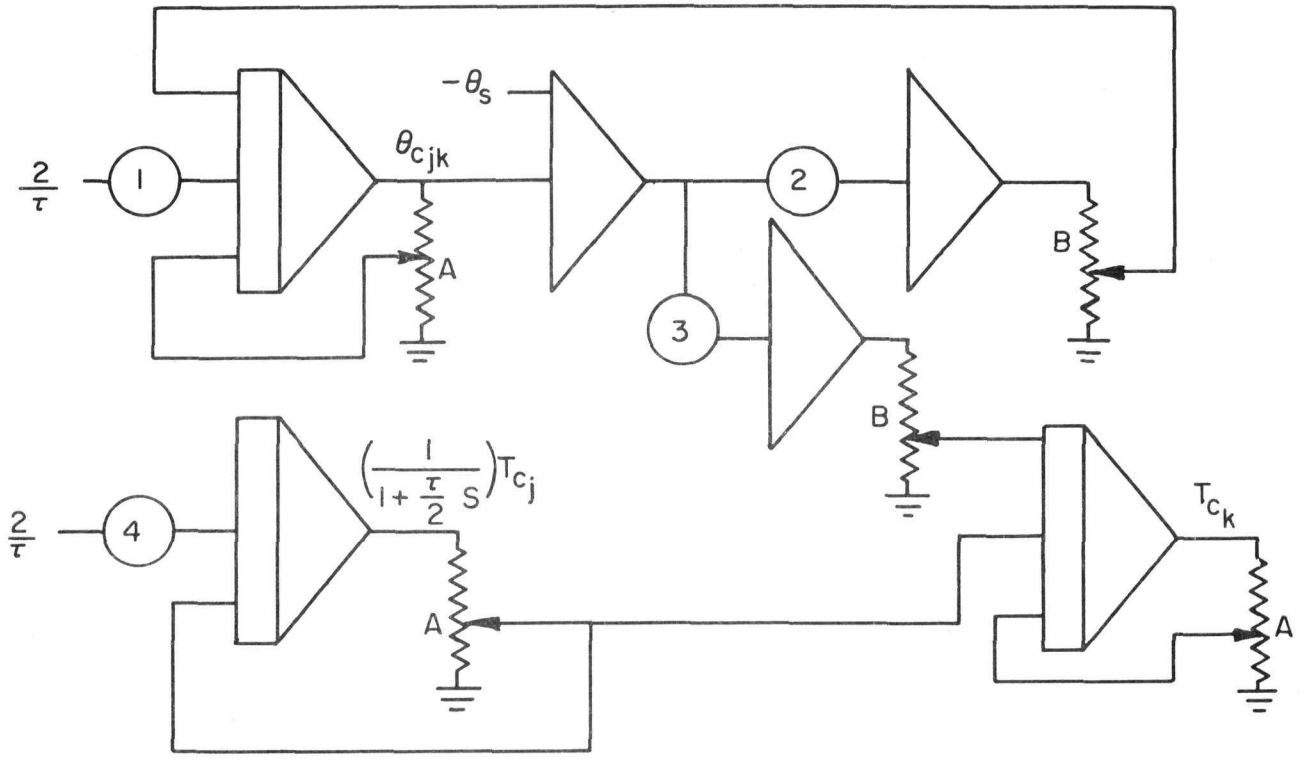

1. T_{c_j}
2. $(Z_2/\tau Z_1)/G_o$
3. $2(Z_2/\tau Z_1)/G_o$
4. $-T_{c_j}$

A. Servo-multiplier cup with a $2/\tau$ input

B. Servo-multiplier cup with a G input

A-28293

FIGURE 22. COMPUTER DIAGRAM FOR REACTOR-COOLANT TEMPERATURES WITH VARIABLE FLOW SIMULATION

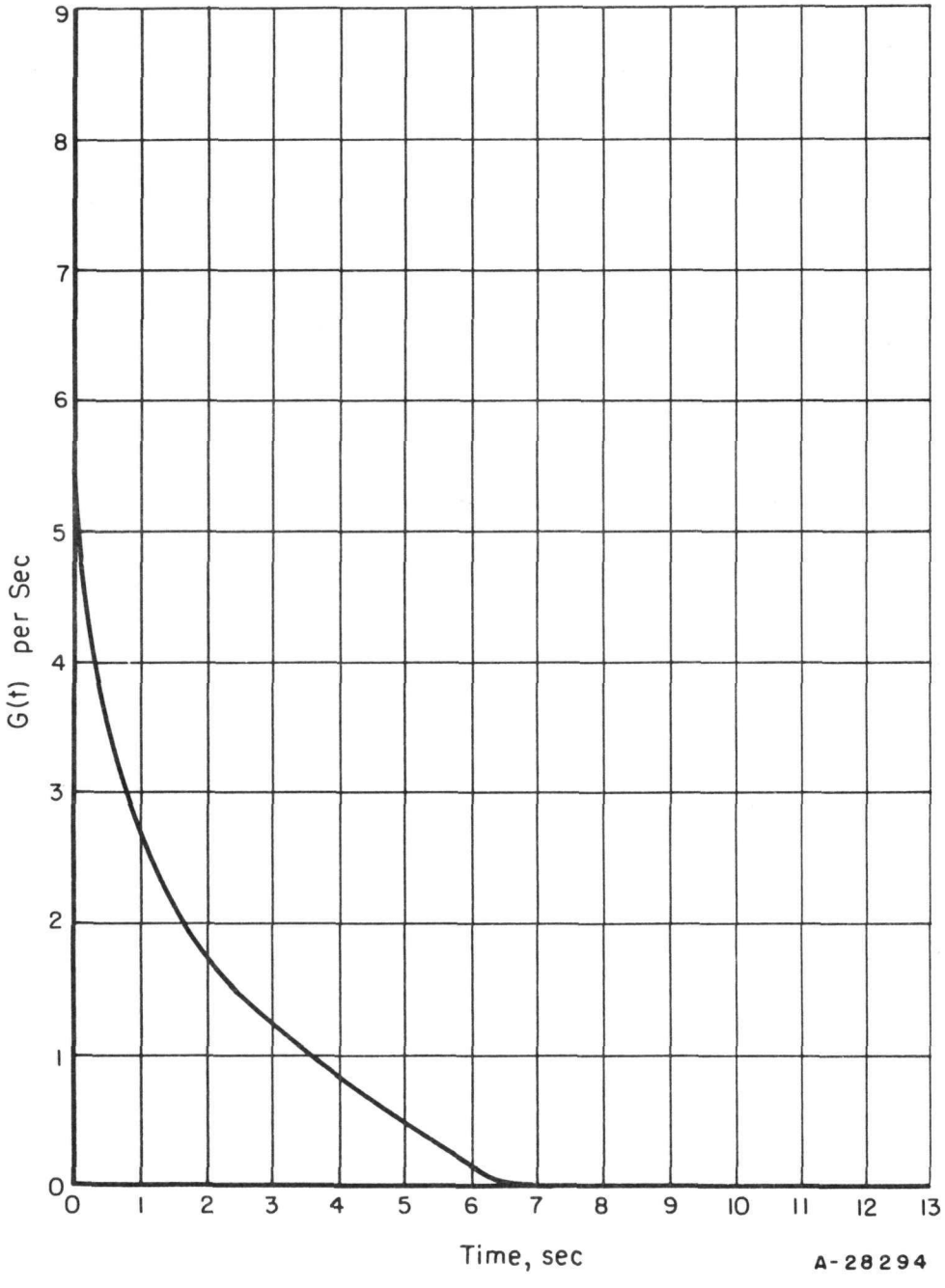

FIGURE 23. HEAT-TRANSFER FILM COEFFICIENT

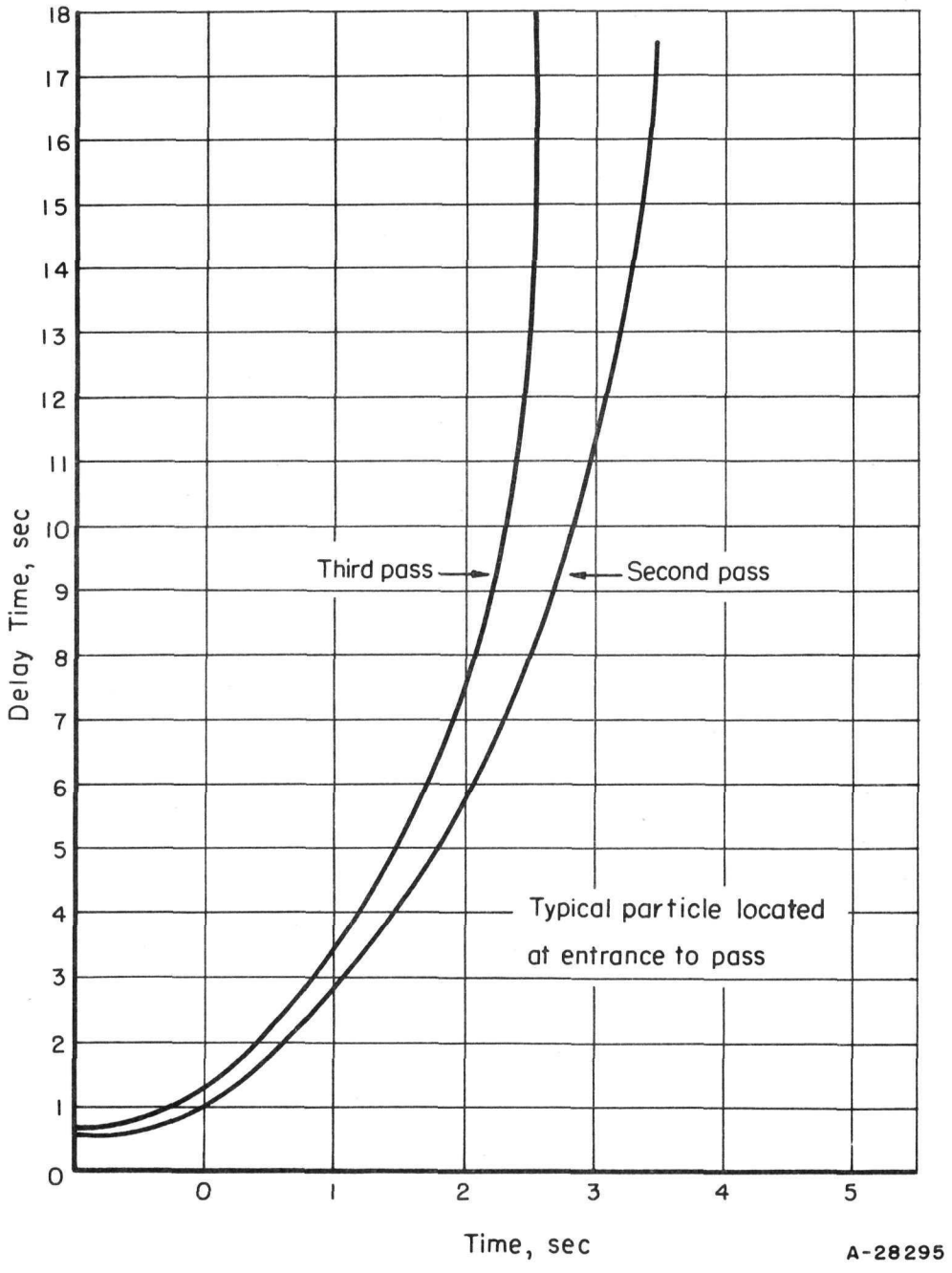

FIGURE 24. COOLANT-TRANSPORT LAG THROUGH REACTOR PASSES

approximation. The heat-transfer coefficient was allowed to decrease normally. The initial temperatures for this case are listed in Table 15.

The coastdown takes place in less than one loop time, so simulation of the primary loop and steam generator was unnecessary.

Program Analysis and Discussion of Loss-of-Flow Accident

The analysis of this accident included variation of the following parameters:

(1) Scram-delay time

(2) Total negative reactivity available for shutdown

(3) Scram rate, negative reactivity versus time

(4) Moderator-temperature coefficient.

A temperature cross section of the fuel pin for the standard four-pump coastdown with no scram is shown in Figure 25. A comparison of P_r, θ_{3_1}, and θ_{s_3} responses, with and without scram, for the four-pump case is presented in Figures 26 through 28. Responses of the two-pump case are similar, but with less excursion.

Loss-of-Flow-Investigation Results

The results of this study indicate that there are no serious consequences from the loss of flow. The equilibrium pin temperature with no scram is about 1100 F, and with scram it is about 820 F. In general, a variation of the scram parameters has little effect on the system. The most critical parameter is the moderator-temperature coefficient. With the maximum rise of coolant temperature of 85 F, δk only changes from -0.0025 to -0.0132. However, with scram, system response is much the same with any value of moderator-temperature coefficient.

For the half-flow case, the transients are even less severe. The corresponding equilibrium pin temperatures are 700 F with no scram, and 600 F with scram. These are average temperatures measured in the third pass.

TABLE 14. INITIAL SYSTEM TEMPERATURES FOR FOUR-PUMP-COASTDOWN CONDITION

Second Pass	Temperature, F	Third Pass	Temperature, F
θ_{2_1}	742	θ_{3_1}	1242
θ_{2_2}	728	θ_{3_2}	1198
θ_{2_3}	701	θ_{3_3}	1108
θ_{2_4}	665	θ_{3_4}	964
θ_{2_5}	620	θ_{3_5}	806
θ_{He_2}	559	θ_{He_3}	637
θ_{s_2}	523	θ_{s_3}	543
θ_{f_2}	673	θ_{f_3}	972
$\theta_{c_{bc}}$	506	$\theta_{c_{de}}$	515
T_{c_b}	495	T_{c_d}	501
T_{c_c}	501	T_{c_e}	517

TABLE 15. INITIAL SYSTEM TEMPERATURES FOR TWO-PUMP-COASTDOWN CONDITION

Second Pass	Temperature, F	Third Pass	Temperature, F
θ_{2_1}	554	θ_{3_1}	691
θ_{2_2}	551	θ_{3_2}	680
θ_{2_3}	546	θ_{3_3}	660
θ_{2_4}	538	θ_{3_4}	626
θ_{2_5}	527	θ_{3_5}	589
θ_{He_2}	515	θ_{He_3}	550
θ_{s_2}	508	θ_{s_3}	530
θ_{f_2}	538	θ_{f_3}	629
$\theta_{c_{bc}}$	499	$\theta_{c_{de}}$	509
T_{c_b}	498	T_{c_d}	503
T_{c_c}	503	T_{c_e}	518

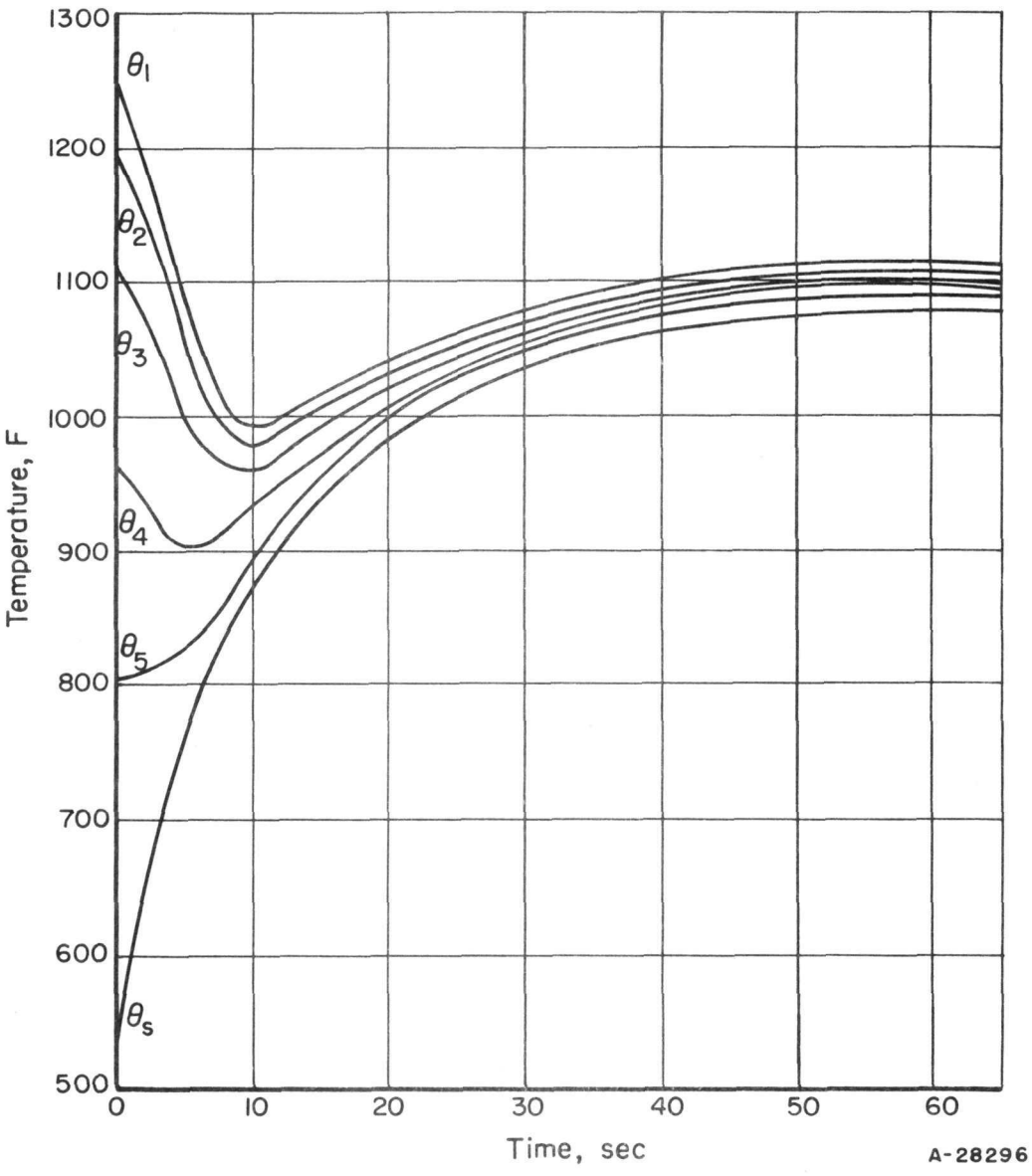

FIGURE 25. TEMPERATURE CROSS SECTION OF THE AVERAGE THIRD-PASS FUEL PIN FOR THE FOUR-PUMP COASTDOWN WITH NO SCRAM

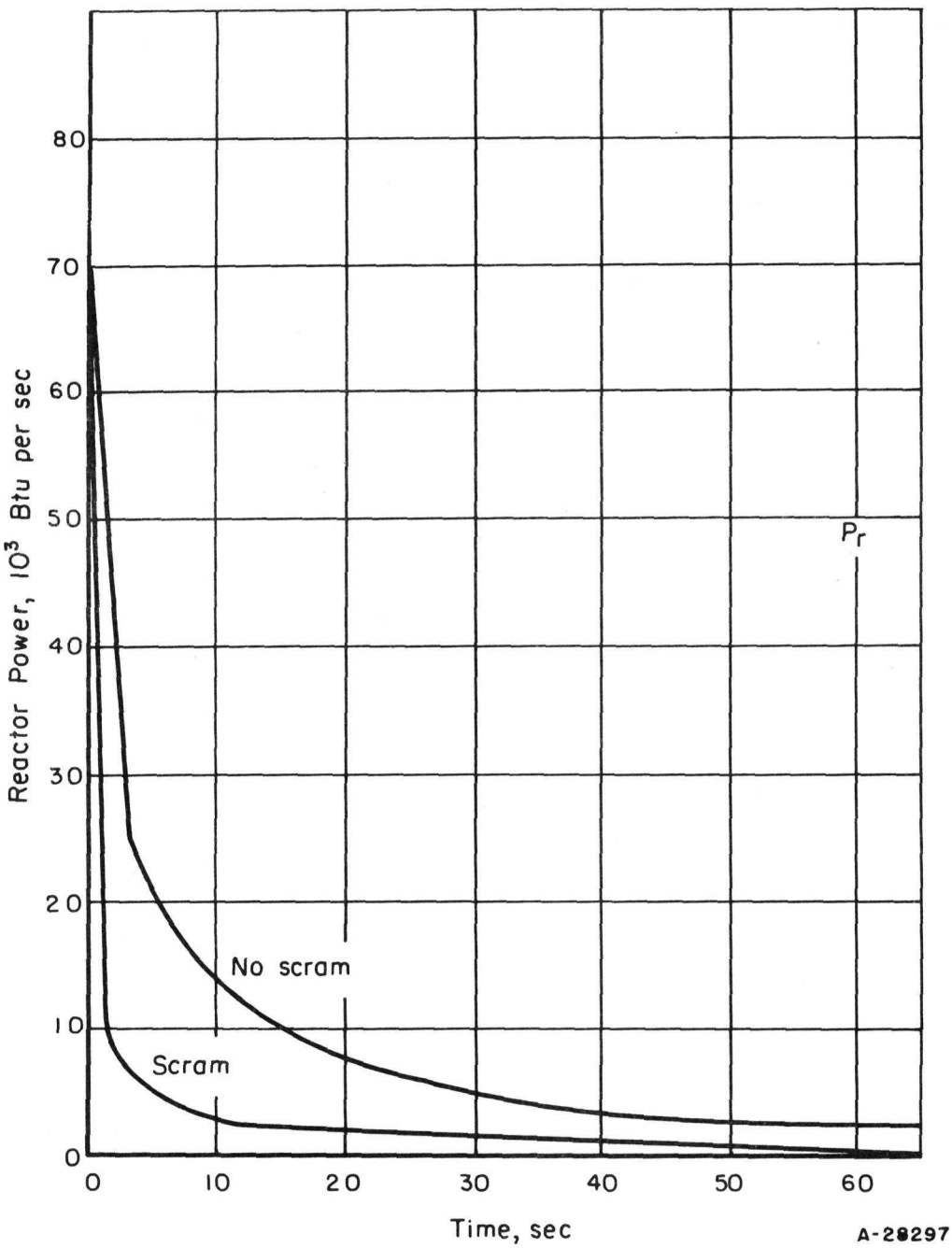

FIGURE 26. REACTOR POWER, FOUR-PUMP COASTDOWN, WITH AND WITHOUT SCRAM

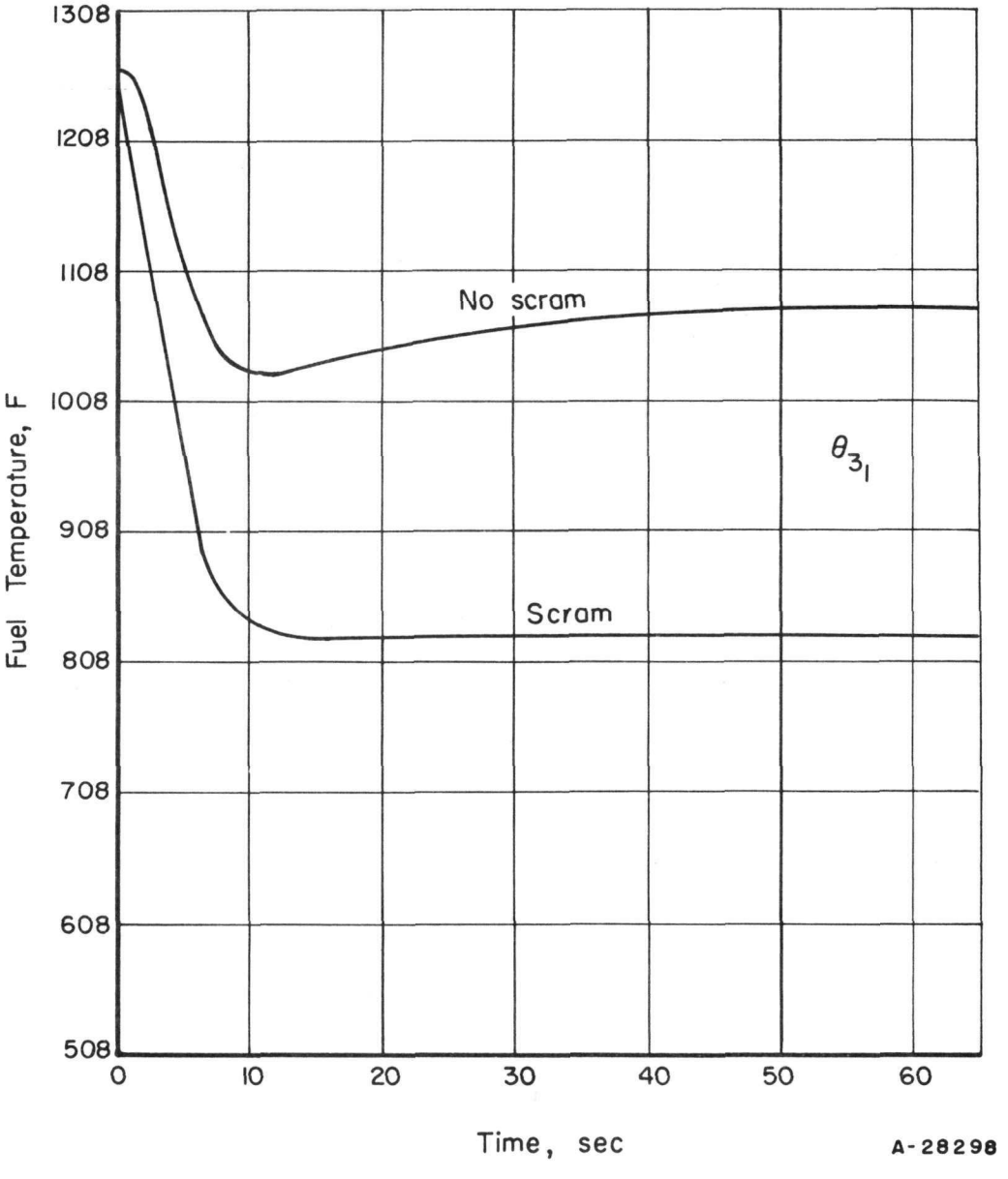

FIGURE 27. CENTER FUEL-PIN TEMPERATURE, FOUR-PUMP COASTDOWN, WITH AND WITHOUT SCRAM

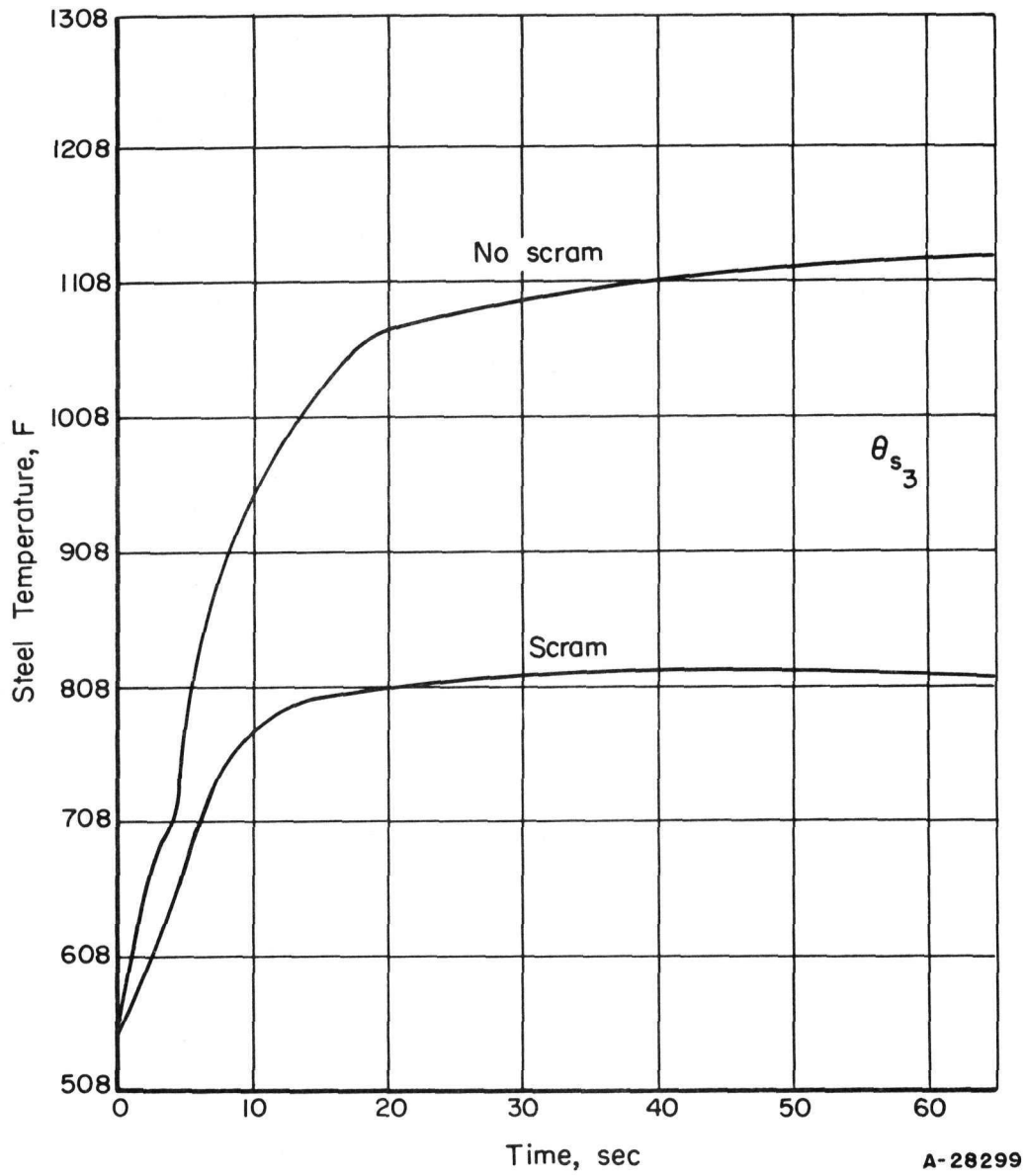

FIGURE 28. STEEL TEMPERATURE, FOUR-PUMP COASTDOWN, WITH AND WITHOUT SCRAM

COLD-WATER ACCIDENT

This accident results from the flow of water from an idle, cool primary loop into the reactor. The colder water introduces excess reactivity because of the negative moderator coefficient, and a fast power rise could result. Since the reactivity change is proportional to the change in temperature and magnitude of the moderator coefficient, it is important to investigate the maximum cold-loop temperatures allowable without endangering the reactor core. This will determine the requirement for safety interlocks and their temperature setting.

Two conditions of flow were considered:

(1) Opening of shutoff valve in cold loop with pumps running

(2) Starting main coolant pumps in the cold loop with shutoff valve open.

The following assumptions were made:

(1) 54 per cent power in hot loop (40 megawatts)

(2) 57.6 per cent initial flow in hot loop

(3) Initial reactor inlet temperature of 492 F

(4) Hot- and cold-loop inlet temperatures constant

(5) Perfect fluid mixing at inlet to reactor.

Figure 29 shows the flow variations of the hot and cold loops for the second condition. Since normal flows occur in less than 2 sec, the flow would reach 100 per cent before any change occurred in inlet temperature at the entrance to the second pass. Thus, only the inlet temperature was considered as a time-dependent variable. This function is shown in Figure 30. Two initial cold-loop temperatures were considered in this study, one at 130 F and the other at room temperature, 70 F.

For the condition of valve opening, the flow was also assumed to reach 100 per cent before the temperature changed at the inlet to the second pass. This is a conservative approximation.

Cold-Water Simulation

Since the change in flow characteristics was neglected for this study, the standard coolant and transport-lag simulations were employed. The period circuit described previously was used for period trip.

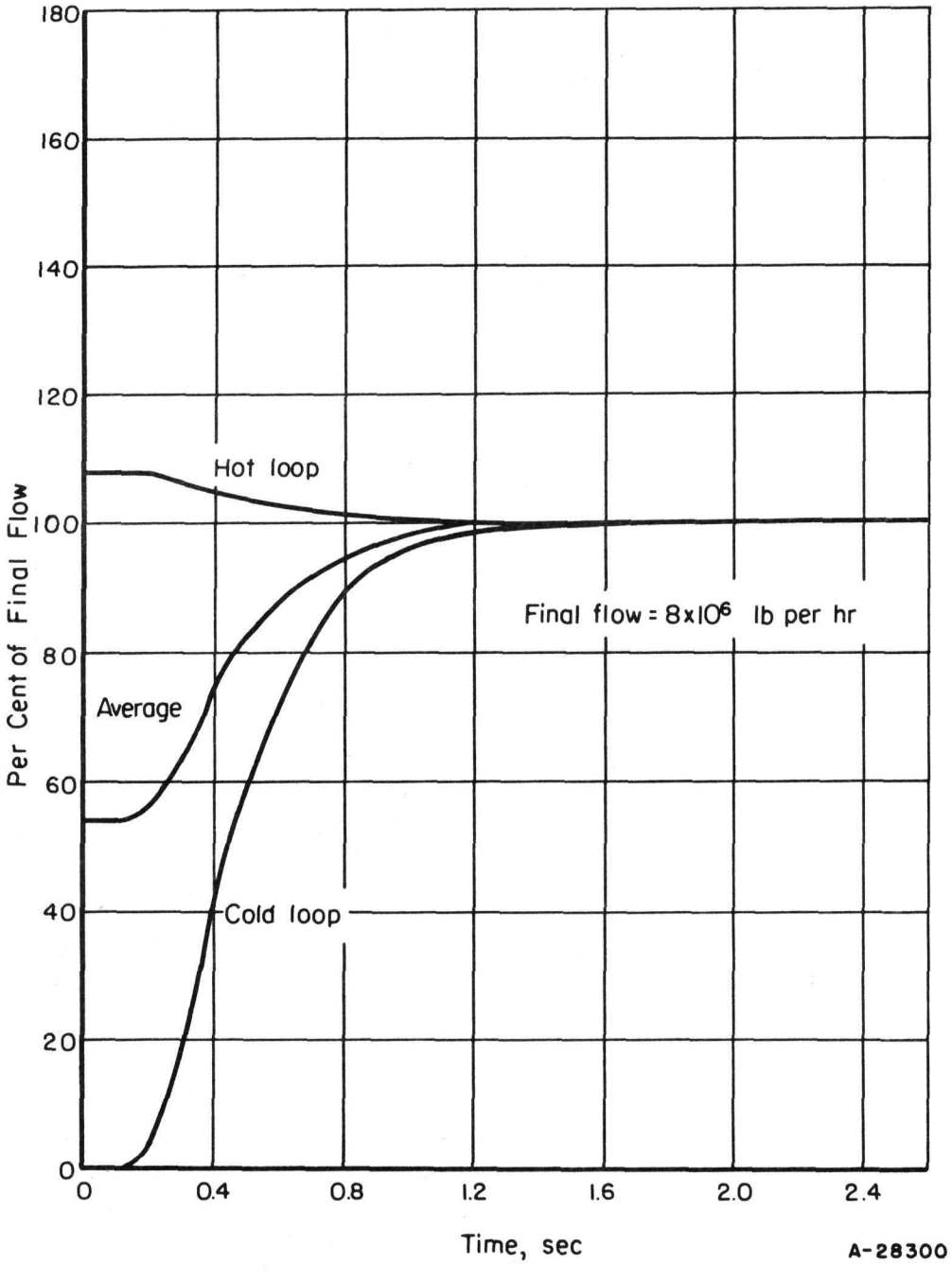

FIGURE 29. COOLANT-FLOW VARIATIONS AFTER IDLE-LOOP STARTUP

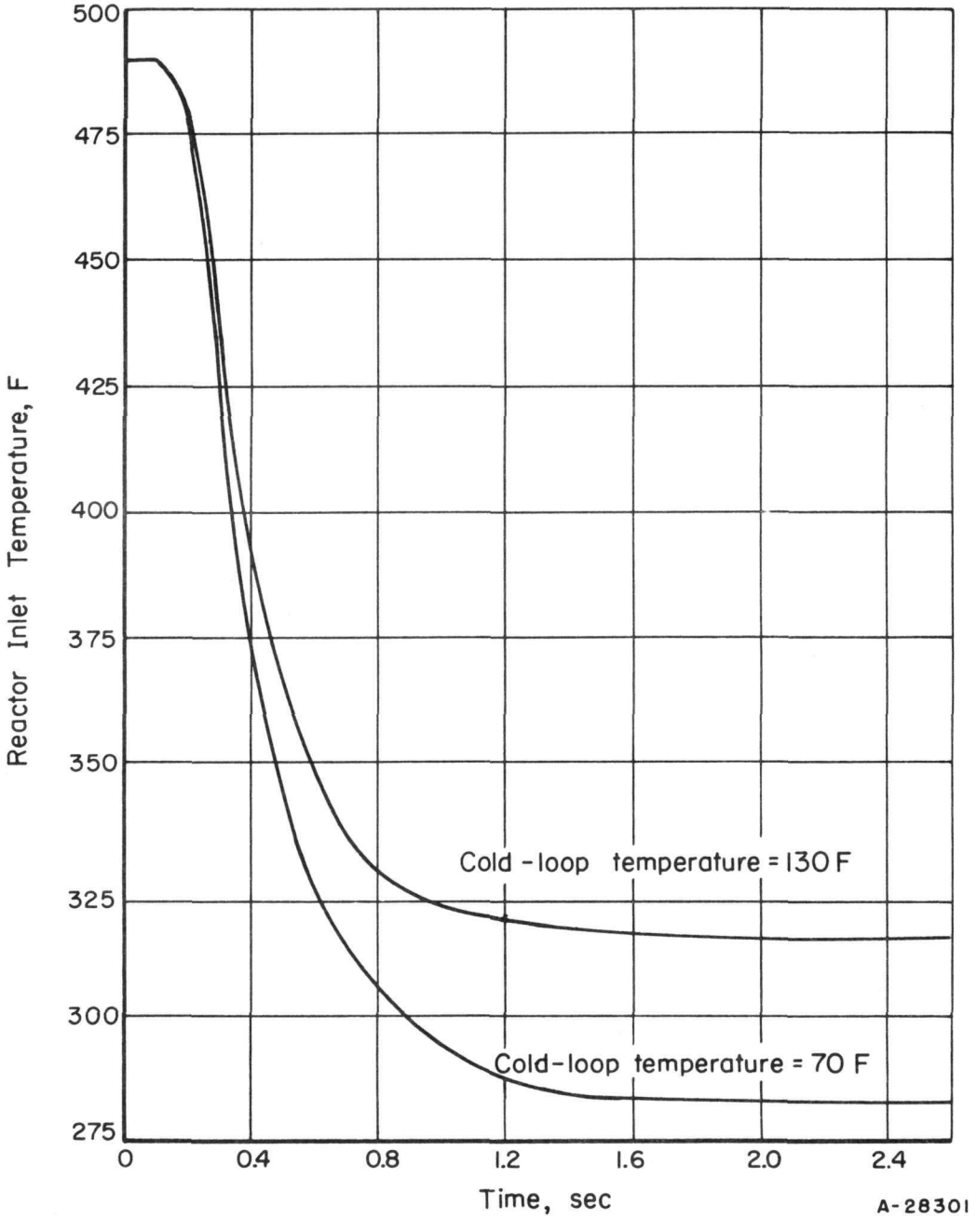

FIGURE 30. REACTOR INLET TEMPERATURE AFTER MIXING OF COOLANT FROM HOT AND COLD LOOPS

Program Analysis and Discussion for Cold-Water Accident

With 70 F and 130 F inlet temperatures, for no safety action, flux trip, and period trip, the following parameter variations were considered:

(1) Moderator-temperature coefficient

(2) Fuel-temperature coefficient

(3) Flux-trip level

(4) Scram-delay time

(5) Period-trip level

(6) Shutdown reactivity.

Figures 31 through 34 show a comparison of the responses of the system for the two cold-loop temperature inputs with all standard scram conditions and flux trip at 55 megawatts.

In the previous accident studies, variation of the parameters had little effect on the response of the system. However, in this study particular variations have a profound effect on the power level and magnitude of temperature excursions.

To show the effects of parametric variations, Table 16 relates the peaks of power level, center-pin temperature, and cladding temperature to the various changes from standard design values of the parameters.

TABLE 16. EFFECTS OF PARAMETER VARIATIONS WITH SCRAM DURING COLD-WATER ACCIDENT FOR PUMP STARTING WITH VALVE OPEN

Parameter	Reactor Power, 10^3 Btu per sec		Temperature, F	
	Second Pass	Third Pass	θ_{3_1}	θ_{s_3}
All standard values	675	835	2150	564
70 F cold-loop temperature	1340	--(a)	2800	574
High moderator coefficient	1180	--(a)	2600	568
Low moderator coefficient	100	15	900	548
Low Doppler coefficient	960	--(a)	3500	578
Trip level at 44 megawatts	200	1550	2250	550
Trip level at 66 megawatts	775	700	2200	568
100-millisecond scram delay	200	1500	2250	550
400-millisecond scram delay	1225	550	2200	576
0.01 shutdown δk	750	--(a)	4050	626
0.10 shutdown δk	415	1	1000	558
10-sec period trip	245	100	2200	580
1-sec period trip	--(a)	65	2200	606

(a) Power exceeded 2500 x 10^3 Btu per sec.

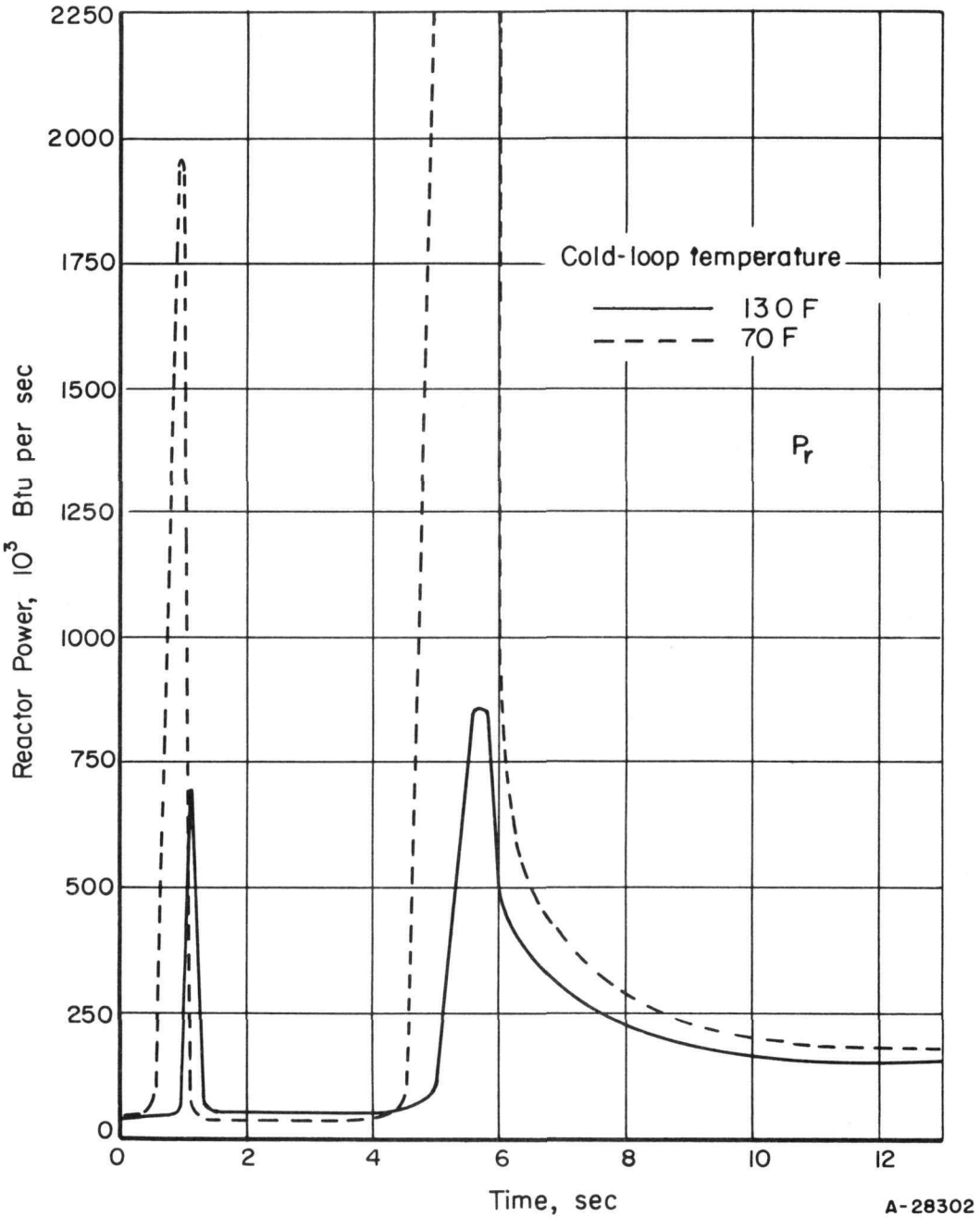

FIGURE 31. REACTOR POWER LEVEL UNDER STANDARD SCRAM PARAMETERS, COLD-WATER ACCIDENT

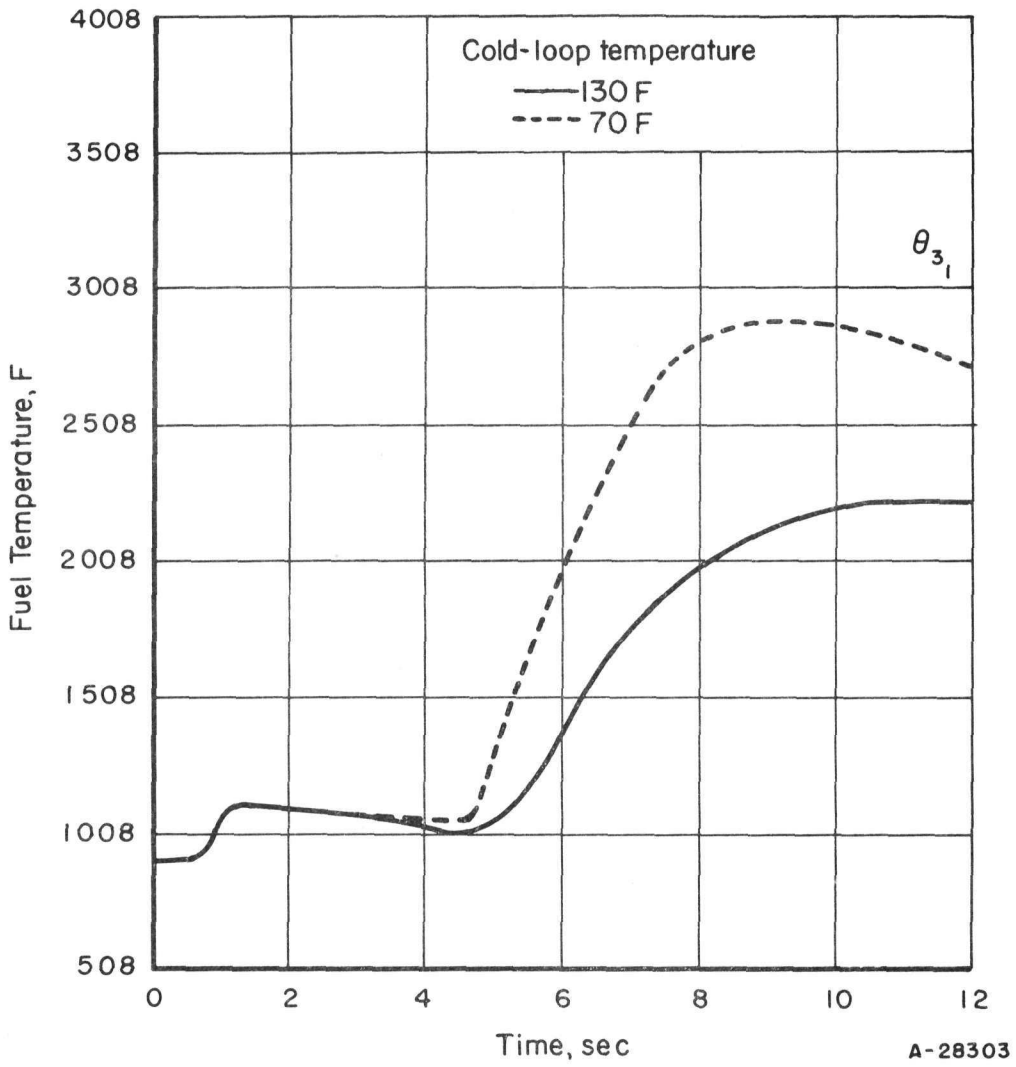

FIGURE 32. CENTER-PIN TEMPERATURE WITH STANDARD SCRAM PARAMETERS, COLD-WATER ACCIDENT

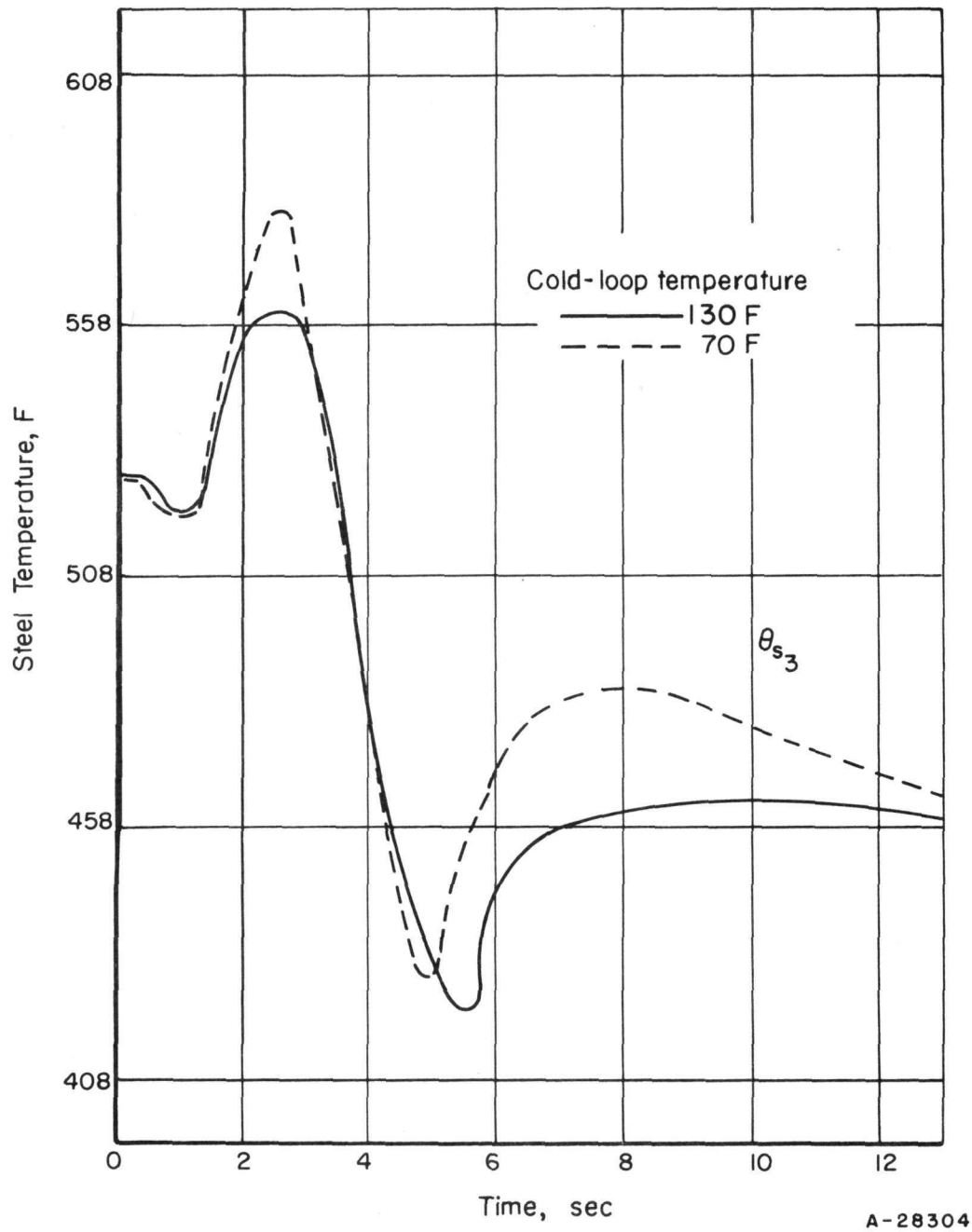

FIGURE 33. STEEL TEMPERATURE WITH STANDARD SCRAM PARAMETERS, COLD-WATER ACCIDENT

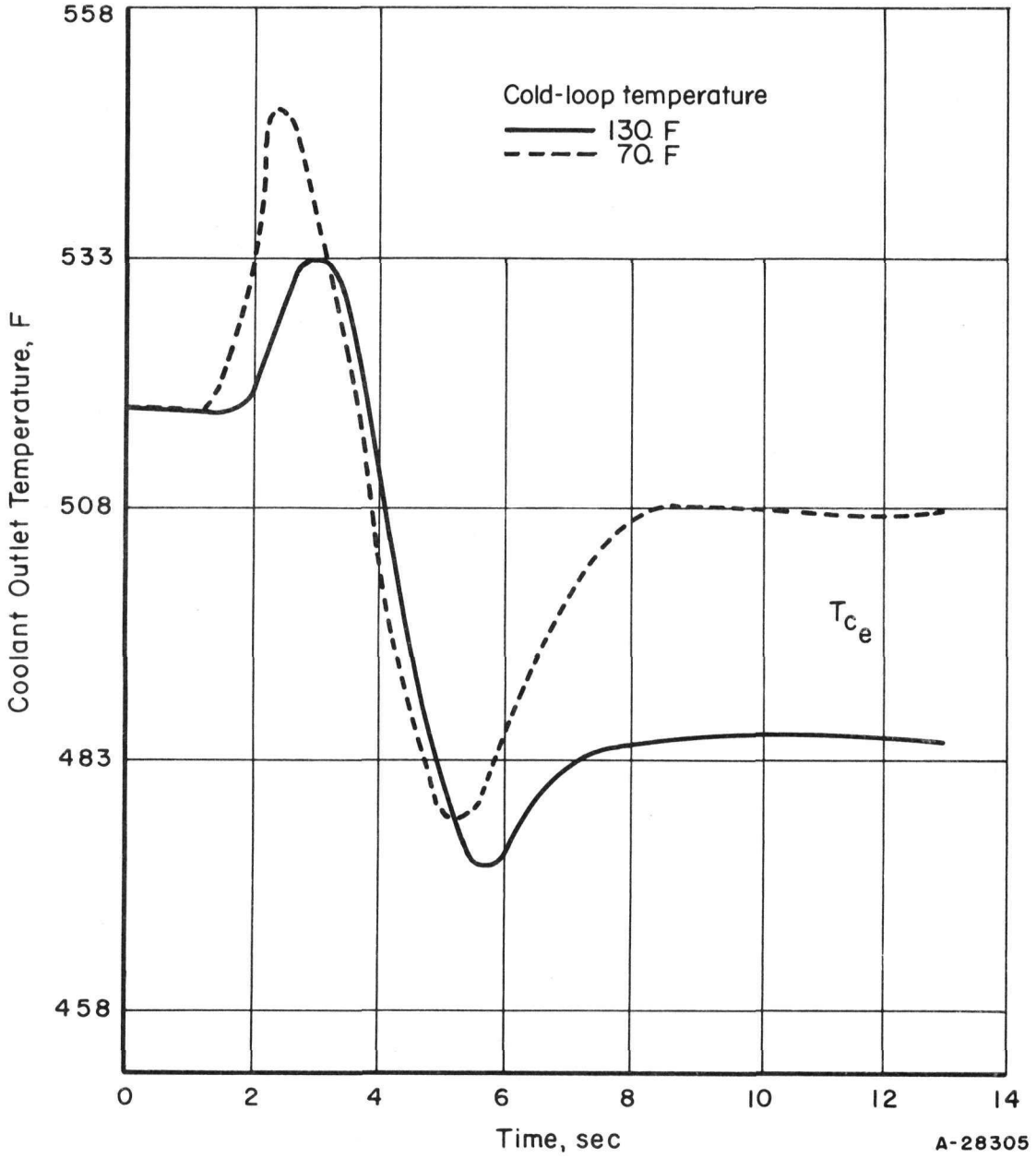

FIGURE 34. COOLANT OUTLET TEMPERATURE WITH STANDARD SCRAM PARAMETERS, COLD-WATER ACCIDENT

It should be noted that the peaks in the above curves correspond to the effects of the entrance of the cool water into the second and third passes.

Cold-Water-Investigation Results

Results of this accident indicate that, in general, with the difference in loop temperatures on the order of 300 F, scram action is necessary. Only in the case with low moderator coefficient was it possible to observe the effects of no scram. The excursions of this run correspond roughly to the case of the 100-millisecond scram-delay run.

The standard case for the idle-loop startup simulation showed power excursions of 250 and 1100 megawatts for the second and third passes along with peak temperatures of 2800 F and 790 F for the center pin and cladding, respectively.

In the case of valve opening with pumps running, the change in inlet temperature was on the order of 35 F per sec, resulting in a less severe accident.

Best results were obtained using the lowest value of the moderator coefficient, as would be expected. For optimum design against the cold-water accident one should have as much shutdown δk available as possible. If sufficient shutdown δk is not available, severity of power and temperature excursions can be minimized by a relatively long delay before scram, such as increased scram-delay time or trip at a relatively high power level. The purpose of the long delay before scram is to allow time for the average fuel and coolant temperatures to increase appreciably before scram occurs. This lowers the Doppler δk, and makes the increase in moderator δk less severe when the cold coolant reaches the third pass. As seen in Table 16, some of these parametric changes result in less excursion in the third pass than in the second.

The safety interlocks should prohibit accidental startup of the idle loop with excessive temperature difference between the loops. Under these conditions the idle loop would have to be preheated.

CONCLUSIONS

The merchant-ship reactor appears to exhibit a high degree of inherently safe operating characteristics. Modification of design parameters specifically for safety considerations is believed to be unnecessary.

For the continuous-rod-withdrawal accident, it is sufficient to stop withdrawal and begin insertion of the rods. If this can be accomplished by other means, scram is not necessary.

The rod-withdrawal rates used in the startup accident produce power excursions which can be checked naturally by means of the Doppler coefficient. Much lower rates would have to be used for startup to limit the period to 3 sec.

The loss-of-flow situation would not cause serious consequences due to the rapid decrease in reactor power. Although the temperature in the average fuel-pin cladding is not excessive, it may be necessary to scram in order to prevent melting of the clad in the "hot channel".

The severity of the cold-water accident depends upon the difference in temperature of the two transport loops. When this difference is on the order of 300 F, scram is mandatory. Best response to scram is obtained with high negative reactivity available for shutdown. If the negative reactivity available for shutdown is insufficient to override the reactivity introduced by the cold water, the power excursion can be reduced by a relatively long delay before scram.

This reactor system appears to respond safely to these particular accident situations.

REFERENCES

(1) Schultz, M. A., Control of Nuclear Reactors and Power Plants, McGraw-Hill Book Company, Inc., New York (1955), pp 176-179.

(2) Hasek, C. W., "Nuclear Merchant Ship Propulsion Plant Status Report", AIF Preprint No. 57-50 (October, 1957).

(3) Stone, J. J., and Mann, E. R., "Oak Ridge National Laboratory Reactor Controls Computer", ORNL-1632 (April 20, 1954).

(4) Cunningham, W. J., "Time-Delay Networks for an Analog Computer", Transactions of the IRE, PGEC, EC-3 (4), 16-18 (1954).

RSB/BBG/RHB/LEW/JJS:bwl